

# Organic Solar Cells and Their Nanostructural Improvement

Serap Günes

**Abstract** Organic solar cells comprised of organic semiconductors have attracted considerable attention in the areas of photonics and electronics during the last decade. Organic semiconductors are a less expensive alternative to inorganic semiconductors. Organic molecules and conjugated polymers as organic semiconductors can be processed by simple techniques that are not available to crystalline inorganic semiconductors. The flexibility in the synthesis of organic molecules allows for the alteration of molecular weight, band gap, energy levels, and structural order, which makes organic semiconductors unique. The conversion of sunlight to electricity by organic solar cells is very interesting and promising since organic solar cells offer the possibility of fabricating large area, light-weight, cost-effective, flexible devices using simple and environmental friendly techniques. Also, organic solar cells can be integrated into wide variety of structures and products in ways not possible for conventional solar cells. As a clean renewable energy source organic solar cells are rapidly developing. A power conversion efficiency over 7–8% was reported recently. However, this value must be improved to compete with conventional solar cells. On the other hand, there is a considerable progress in the evolution of organic solar cells from pure scientific research to a possible industrial application. Recent efforts are devoted to the investigation of operating mechanisms, new synthesis routes, new device architectures, stability of the organic materials, lifetime, encapsulation, etc. If comparable or even slightly lower efficiencies than those of conventional technologies can be achieved, the cost-effectiveness and versatility of organic compounds will make organic solar cells more favorable. In this chapter, an overview on principles of operation, critical parameters, nanomorphology, charge transport and mobility,

---

S. Günes (✉)

Faculty of Arts and Science, Department of Physics, Davutpasa Campus,  
Yildiz Technical University, 34210, Esenler, Istanbul, Turkey  
e-mail: sgunes@yildiz.edu.tr

stability, possible routes for improvement, and the recent status and future aspects of organic solar cells will be discussed.

## 1 Introduction

A solar cell converts sunlight into electricity. Harvesting energy directly from sunlight using photovoltaic (PV) technologies is a viable way to eliminate the disadvantages of decreased availability of fossil fuel sources and the long-term effects of CO<sub>2</sub> emission. The recognition of the potential of PV technology led to the rapid growth of production of terrestrial solar cell modules [1]. Current production is highly dominated by crystalline silicon (Si) modules, which represent 94% of the market. A maximum theoretical power conversion efficiency (PCE) of almost 31% under direct air mass (AM) 1.5 sunlight is expected for silicon-based devices [1, 2]. Although the industry is currently based on Si, significant material challenges and high manufacturing costs might not allow Si-based devices to meet the long-term goals of PV technology. Thus, new high efficiency or low-cost technologies such as multi-junction and organic-based devices are rapidly growing [1]. Organic photovoltaics (OPV) have the potential for low-cost device production.

An organic solar cell consists of an organic layer which realizes the basic steps in PV conversion such as light absorption, charge carrier generation, charge carrier transport and extraction or injection of charge carriers through the contacts [3]. PV cells based on organic compounds have potential cost-effectiveness, flexibility, and easy processing [4]. Two main approaches have been considered in the research of OPVs: bulk heterojunction (BHJ), which is represented in an ideal case as a bicontinuous composite of donor and acceptor phases [5, 6], and donor-acceptor bilayers achieved by vacuum deposition of organic molecules [7, 8].

BHJ type devices employ conjugated polymers which can be solution processed. This is seen as an advantage over the vacuum deposition since processing in solution gives the ability to process the active layer from solution in a single step using various techniques such as ink jet printing, spin coating, and roller casting [9]. In polymer-based BHJ solar cells, which are achieved by blending a polymer donor and acceptor, the most common donor polymers are poly[2-methoxy-5-(3,7-dimethyloctyloxy)-1,4-phenylene vinylene] (MDMO-PPV) [10, 11], regioregular poly(3-hexylthiophene) (RR-P3HT) [12–16], and poly[2-methoxy-5-(2'-ethylhexyloxy)-1,4-phenylene vinylene] (MEH-PPV) [17–19]. The most widely used acceptor material of choice has been [6,6]-phenyl C<sub>61</sub>-butyric acid methyl ester (PCBM) [20]. Several small organic materials, such as zinc phthalocyanine (ZnPc) [21, 22] and copper phthalocyanine, [23] have also been used as donors in bilayer heterojunction solar cells.

Optimized organic devices have PCE of 5–8% [24–26]. Although there has been significant improvement in organic solar cell PCEs, they still have not

reached that of conventional solar cells [27]. In order to compete with the conventional inorganic cells, a PCE of more than 10% is desirable [4, 28–31]. Various approaches to organic solar cell designs have been employed such as using novel organic materials [16, 32] or a combination of organic and inorganic (hybrids) [33, 34] as active layer materials, tandem cells [35] and also, various techniques have been employed to improve the performance of organic solar cells such as low band gap polymers [36, 37] polymer–polymer blends [38, 39], new device structures [40], etc. Improving the PCE is the primary interest of the current research on organic solar cells. The efficiencies can be further improved by tailoring the materials and also engineering of the device structures. However, one should note that stability and life times are also important issues [41, 42].

In this chapter, an overview of basic operation principles, organic solar cell materials, and possible routes for performance improvement of organic solar cells will be overviewed.

## 2 Basics of Organic Photovoltaics

### 2.1 Organic Photovoltaic Materials

Research on organic solar cells focuses on two types of materials: one is solution processed, such as semiconducting polymers/molecules, and the other is vacuum processed, such as small organic molecules. Polymers decompose under excessive heat and have too large molar mass for evaporation. Therefore, most polymer-based PV elements are solution processed at low temperatures [43].

The discovery of conducting polymers opened up a way of achieving a new generation of polymers: materials that exhibit the electrical and optical properties of metals or semiconductors and retain the attractive mechanical properties and processing advantages of polymers [44]. Saturated polymers in which all of the four valence electrons are used up in covalent bonds are not very interesting as electronic materials since they are insulators. However, in conjugated polymers the electronic configuration is fundamentally different. The chemical bonding in conjugated polymers leads to one unpaired electron (the  $\pi$  electron) per carbon atom and  $\pi$  bonding leads to electron delocalization along the back bone of the polymer which provides the “high way” for charge mobility along the backbone of the polymer chain. The chain symmetry such as the number and kind of atoms within the repeat unit determines the electronic structure in conducting polymers. As a result, such polymers can exhibit semiconducting or even metallic properties [44]. Materials that have an extended delocalized  $\pi$  electron system can absorb sunlight and create photogenerated charge carriers and also transport these charge carriers, which makes them interesting as optoelectronic materials [43]. Conjugated polymers have become the materials of choice not only for solar cells but also for various optoelectronic applications, such as light emitting diodes (OLEDs) [45–47] and field-effect transistors (OFETs) [48, 49].

Organic materials for use in PV devices require a good chemical stability and high optical absorption in the visible range with respect to the AM1.5G spectrum [50]. Efficiencies of the first hole conducting polymers based on conjugated polymers were less than satisfactory [51]. Previously, higher efficiencies were achieved by switching to different classes of donor type conjugated polymers and by mixing them with suitable electron acceptors like fullerenes [52–56]. High performance organic solar cells employ polymer-fullerene blends in which the polymer acts as a donor whereas the fullerene acts as an acceptor. The Buckminsterfullerene,  $C_{60}$ , is a strong acceptor. A soluble derivative of  $C_{60}$ , namely PCBM (1-(3-methoxycarbonyl) propyl-1-phenyl [6,6]  $C_{61}$ ), which has been widely used in polymer/fullerene solar cells due to its solution processability owing to their side-chain substitution was synthesized by Wudl et al. [57]. Currently, a PVC of 7.4% is reported. The main reason for the increase in the performance is the much greater absorption of  $C_{70}$  in the visible region relative to that of  $C_{60}$ . The high symmetry of  $C_{60}$  renders low-energy transitions formally dipole forbidden which results in a weak absorption of light in the visible region [9].  $C_{70}$  has an asymmetric structure with significantly stronger absorption across the visible range [11].

Most semiconducting polymers are hole conductors (electron donors). Important representatives of hole conducting donor-type semiconducting polymers are derivatives of phenylene vinylene backbones such as poly[2-methoxy-5-(3,7-dimethyloctyloxy)]-1,4-phenylenevinylene (MDMO-PPV), thiophene chains such as poly(3-hexylthiophene) (P3HT) and fluorene backbones such as (poly(9,9'-dioctylfluorene-co-bis-N,N'-(4-butylphenyl)-1,4 phenylenediamine) (PFB) and PCDTBT. Light harvesting by PCDTBT is better than that of P3HT due to its smaller band gap.

Phthalocyanine and perylene have commonly found applications in thin-film organic solar cells [58]. Phthalocyanine is a representative of the *p*-type, hole conducting materials that work as electron donors, whereas perylene and its derivatives show *n*-type, electron conducting behavior, and serve as the electron acceptor materials. Small organic molecule semiconductors are generally suitable for evaporation/sublimation techniques since their solubility in common organic solvents is limited. Fig. 1.

## 2.2 Operation Principles

There are four important steps for the conversion of solar illumination into photocurrent in organic solar cells: (i) absorption of a photon to create an exciton, (ii) diffusion of the exciton to a donor–acceptor interface, (iii) charge transfer of an exciton into an electron in the acceptor and a hole in the donor, and (iv) collection of the charges at the electrodes [59].

The absorption spectrum of the organic material defines the spectral range over which the cell will respond to light. This depends on the chemical structure of the polymer or molecule. Most organic dyes or molecules are strongly absorbing and a

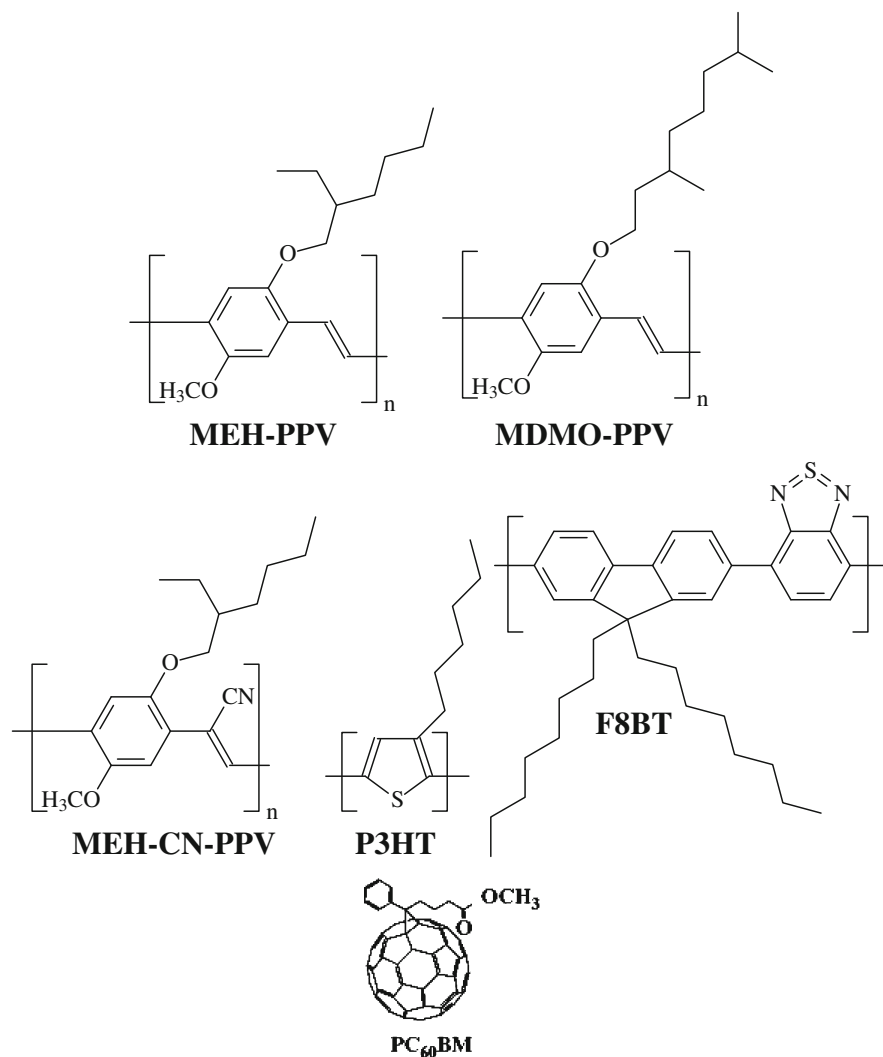
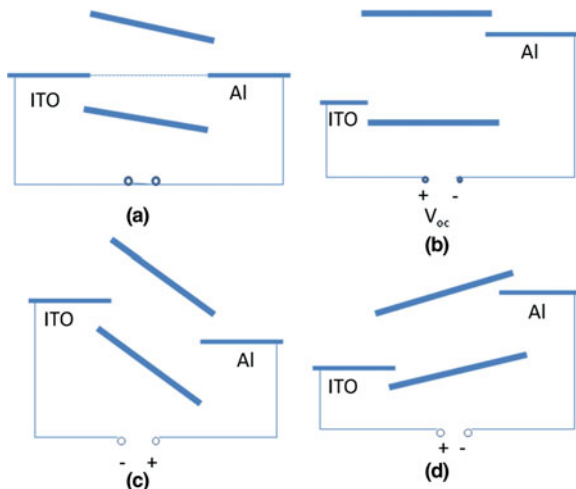


**Fig. 1** Some examples of the representative donors and acceptors used in organic solar cells

film only a few 100 nm thick is sufficient to absorb significant proportion of light if it falls within the absorption band of the material [60]. The first process in photoconversion is related to the absorption. The absorption efficiency is governed by the absorption spectra of the organic semiconductors, their thickness and also, the device architecture.

In organic semiconductors, optical excitations lead to electron-hole pairs (excitons) that are bound at the room temperature [61]. The efficiency of exciton diffusion in organic solar cells is determined by the exciton diffusion length and

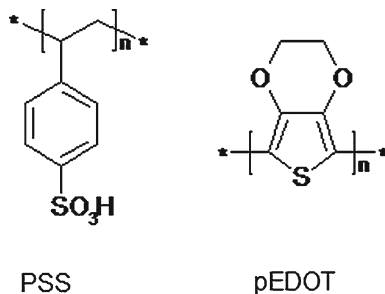
**Fig. 2** Metal-insulator–metal (MIM) models of an organic diode: **a** short circuit, **b** open circuit, **c** reversed bias, and **d** forward bias



the morphology of the donor–acceptor interface [59]. Once excitons are created they can diffuse over a length of approximately 5–15 nm [62–64]. Then they decay either radiatively or non-radiatively. Excitons must be separated into free charge carriers within their lifetime for PV purposes. For efficient dissociation of excitons, strong electric fields are utilized, via externally applied fields or via interfaces. At an interface where abrupt changes of the potential occur, there are strong local electrical fields possible ( $E = -\text{grad } U$ ) [65]. Here, excitons can dissociate into an electron in one phase and a hole in the other. Exciton dissociation can also occur at bulk trap sites, leading to one trapped carrier and one potentially free carrier [66, 67]. Conversion of the excess photon energy above singlet exciton into the vibrational heat bath of a polymer segment is also considered a main source of the energy required for charges to escape from a potential well formed by a superposition of the Coulomb and external electric fields [68].

Once, the electrons and holes are separated, and the free charge carriers are created, these free charge carriers are transported to the electrodes [69]. To understand the rectifying behavior of a semiconductor device, the metal–insulator–metal (MIM) model is used. In Fig. 2, a single layer cell with ITO and Al electrodes is shown. Figure 2a shows the short-circuit conditions. The current delivered by a solar cell under zero bias is called the short-circuit current ( $I_{sc}$ ). In the MIM picture, the built-in potential is equal to the difference in the work functions of the metal electrodes. Exciton dissociation and charge transport are driven by the built-in potential. Figure 2b shows the open-circuit case. The voltage where the current equals to zero is called open-circuit voltage ( $V_{oc}$ ).  $V_{oc}$  is equal to the difference between the metals’ work functions and balances the built-in potential. Thus, the current is zero since there is no net driving force acting on the charge carriers. Figure 2c shows the negative bias case. The diode works as a photodetector. Under illumination, the charge carriers drift to the appropriate electrodes. Figure 2d shows the forward bias

**Fig. 3** Chemical structure of PEDOT and PSS



case. In the case of an applied forward bias larger than the  $V_{oc}$  the contacts start injecting charges into the semiconductor. If these charges recombine radiatively, the diode works as a LED.

### 2.3 Device Architecture

As substrates, transparent and conducting electrodes (for example, glass or plastic covered with indium-tin-oxide (ITO)) are used. As a transparent conductive electrode ITO allows light to pass through the cell. However, ITO is not the ideal conductive material due to the following problems: release of oxygen and tin into the organic layer, poor transparency in the blue region and complete crystallization of ITO films, which requires high-temperature processing [70, 71]. Also, the increasing cost of indium prevents large-scale use of ITO in low-cost PV devices [70]. Therefore, alternatives for ITO electrode such as carbon nanotube network electrodes are being investigated [72].

The substrate electrode can be structured by etching. On the transparent conducting substrate, PEDOT:PSS, poly(ethylene-dioxythiophene) doped with polystyrene-sulphonic acid is commonly coated from an aqueous solution. This PEDOT:PSS layer improves the surface quality of the ITO electrode (reducing the probability of shorts) and facilitates hole injection/extraction. Furthermore, the work function of this electrode can be changed by chemical/electrochemical manipulation of the PEDOT layer [73]. PEDOT:PSS is the most promising organic-based electrode material (see Fig. 3) and currently, various modifications of PEDOT:PSS with even greater conductivities are being investigated as electrodes for organic devices [70, 74–76].

As already mentioned, there are two major classes of organic semiconductors: low molecular weight materials and polymers. They have in common a conjugated  $\pi$  electron system formed by the  $p_z$  orbitals of  $sp^2$  hybridized C atoms in the molecules. Compared to the  $\sigma$  bonds that form the backbone of the molecules, the  $\pi$  bonding is significantly weaker. Therefore, the lowest electronic excitations of conjugated molecules are the  $\pi$ - $\pi^*$  transitions with an energy gap leading to light absorption or emission in the visible spectral range [77]. An important difference

between two classes of materials lies in the way they are processed to form thin films. Small organic molecules are usually deposited by sublimation or evaporation whereas conjugated polymers can only be processed from solution by using spin coating or printing techniques [77]. Side chain functionalization is principally used for processing of semiconducting polymers from solution in organic solvents or from water [44]. The active layers are then coated depending on the class of the semiconductor employed in the device. Spin coating, doctor blading, screen printing, and ink jet printing are the most common wet processing techniques. Evaporation of two or more organic molecules at once is called coevaporation and it can be applied to small molecules to create interpenetrating donor–acceptor networks or to achieve molecular doping [78, 79].

The top electrode is, in general, a metal with an underlayer of ultrathin lithiumfluoride. The exact nature of this LiF underlayer is unknown, but certainly such thicknesses (ca 0.6 nm) cannot form a closed layer. The exact role of the LiF underlayer is under controversial debate in the literature [80–82]. Photoelectron spectroscopy studies showed that the metal workfunction can be considerably reduced by evaporation of such LiF layers [83].

The most widely used device configurations in organic solar cells are summarized below.

### 2.3.1 Single Layer Organic Solar Cells

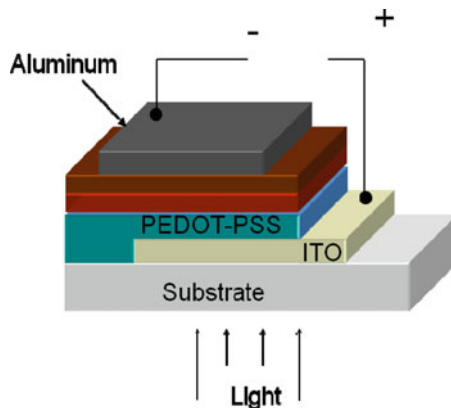
The first organic solar cells were based on single layers sandwiched between two metal electrodes of different work functions. One of the electrodes must be (semi-) transparent, generally ITO, but a thin metal layer can also be used. The other electrode is generally aluminium (calcium, magnesium, gold and others are also used).

Photoexcitations in an organic semiconductor lead to formation of bound electron–hole pairs (excitons). Excitons created in an organic semiconductor must dissociate into free charge carriers according to the PV requirements. The only way to break apart the excitons in the devices consisting of pristine polymers is to use an electric field [84]. If the organic semiconductor is doped, band bending can occur, leading to a Schottky contact at the metal–electrode interface. As a result of the limited exciton diffusion length, only photoexcitations generated close to the depletion region of the Schottky contact can lead to separated charge carriers. Therefore, only a small region contributes to photocurrent generation in pristine polymer-based devices.

The early efforts to realize organic solar cells using conjugated polymers focused on polyacetylene [85] and polythiophene [86]. Previously, visible light emission was observed at Schottky diodes made from semiconducting polymers [45, 87]. The observation of a dual-function device, both as a light emitting diode and a photodiode under reverse bias, using poly[2-methoxy-5-(2'-ethyl-hexyloxy)-1,4-phenylene vinylene] (MEH-PPV) made PPV a material of interest in single-layer organic optoelectronics [88]. However, the PCE of ITO/PPV/Al based



**Fig. 4** Bilayer heterojunction configuration of organic solar cells



devices were reported as 0.07 for light intensities of  $1 \text{ mW/cm}^2$  [89]. The intrinsic field created by the asymmetry of the work function of electrodes was not large enough to generate significant power. Single-layer conjugated polymer-based devices lacked a significant PV effect.

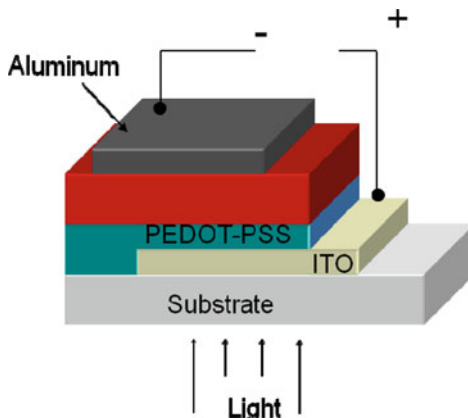
The device architecture plays an important role in the overall efficiency of organic solar cells. In a single-layer device, since only a small region contributes to the photocurrent generation, the efficiency of such devices is rather low [90].

### 2.3.2 Bilayer Heterojunction Organic Solar Cells

The major problem in single-layer organic solar cells is inefficient charge generation in conjugated polymers. To overcome this limitation, the donor/acceptor approach has been suggested [91]. A bilayer device is prepared by stacking a donor and an acceptor material (see Fig. 4). The effective interaction between the donor and the acceptor takes place at the geometric interface in the bilayer heterojunction organic solar cells. Many conjugated polymers in their undoped, semiconducting states are electron donors upon photoexcitation [91]. The photo-physics studies on conjugated polymers and fullerenes reveal that there is ultrafast, reversible and metastable electron transfer from conjugated polymers to Buckminsterfullerenes in solid films [18, 52–54].

Several devices have been constructed using this effect [18, 58]. Tang et al. demonstrated PV activity in small molecular bilayers that were vacuum deposited [58]. They fabricated bilayer organic solar cells by vacuum depositing copper phthalocyanine and a perylene tetracarboxylic derivative. A PCE of about 1% was achieved under simulated AM2 illumination. A novel feature of this device was that the charge-generation efficiency was relatively independent of the bias voltage, resulting in cells with fill factor values as high as 0.65. The interface between the two organic materials, rather than the electrode/organic contacts, was found to be crucial in determining the PV properties of the cell [58]. In a study by

**Fig. 5** Bulk heterojunction configuration of organic solar cells



Yamashita et al. the characteristics of a bilayer heterojunction diode consisting of  $C_{60}$ /tetratriafulvalene (TTF) were reported. The device under dark conditions was almost insulative, however, upon light illumination, remarkable rectification was observed [92]. Halls et al. measured the PV properties of heterojunctions consisting of a layer of the molecular pigment bis(phenethylimido)perylene, sublimed onto a film of the conjugated polymer poly(*p*-phenylenevinylene) [PPV], and sandwiched between electrodes of ITO and aluminum. Quantum yields (electrons collected per incident photon) of up to 6%, fill factors of 0.6 and open-circuit voltages approaching 1 V were obtained, representing significant improvements over single-layer PPV devices [93]. Efficiencies of 3.6% were reported for vacuum-deposited copper phthalocyanine/ $C_{60}$  thin-film double-heterostructure PV cells incorporating an exciton-blocking layer (EBL) [94].

Although significant improvement compared to single-layer devices was achieved in bilayer heterojunction solar cells, the PVC of bilayer heterojunction solar cells is limited due to the following reasons: (i) Efficient charge separation occurs only close to the donor/acceptor interface whereas the photoexcitations far from the donor/acceptor heterojunction will recombine and (ii) PV conversion efficiency is limited by the amounts of photons absorbed in the region where charge separation takes place [91].

### 2.3.3 Bulk Heterojunction Organic Solar Cells

In a bulk heterojunction organic solar cell, donor and acceptor components are mixed to form an interpenetrating network at the nanometer scale (see Fig. 5). The bulk heterojunction concept maximizes the donor–acceptor contact area. If the phase separation between the donor and the acceptor can be controlled to form an interpenetrating network through the control of morphology a high interfacial area within a bulk material can be achieved [91].

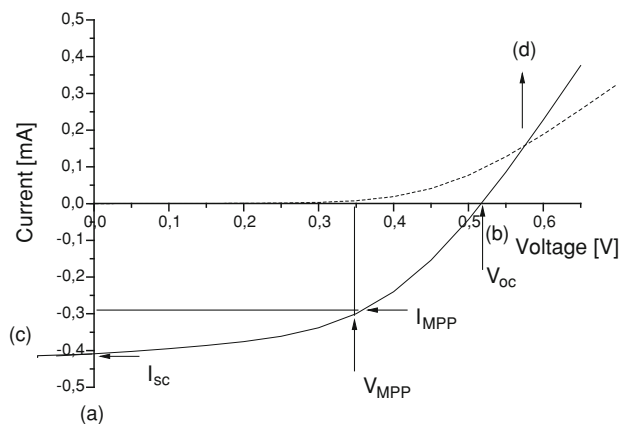


**Fig. 6** Current–voltage ( $I$ – $V$ ) curves of an organic solar cell (*dark, dashed; illuminated, full line*)

Early studies focus on polymer–fullerene bulk heterojunction solar cells. The bulk heterojunction is presently the most widely used photoactive layer. One of the most promising combinations of materials is a blend of a semiconducting polymer and a fullerene derivative as the acceptor.

The study by Shaheen et al. was a breakthrough on bulk heterojunction solar cells with efficiencies reaching 2.5% under simulated AM1.5G illumination using MDMO-PPV as a donor and PCBM as an acceptor. In these cells, the photoactive layer was sandwiched between two electrodes with different work functions. Since then several studies on the morphology, electronic structure, and charge transport of MDMO-PPV/PCBM-based devices were performed [95–100].

P3HT has been another choice of material as a donor in bulk heterojunction cells. The high charge carrier mobility and lower band gap compared to MDMO-PPV make this material advantageous over MDMO-PPV. P3HT/PCBM blends provided an increased PV performance as compared to MDMO-PPV/PCBM solar cells [14, 101]. Recently, 5% efficiency has been achieved using P3HT as the donor and PCBM as the acceptor. By introducing a  $\text{TiO}_x$  layer as the optical spacer they were able to achieve polymer solar cells with PCE approximately 50% higher than similar devices fabricated without an optical spacer [102].

## 2.4 Current–Voltage Characteristics of an Organic Solar Cell

The characteristic parameters of an organic solar cell can be deduced from current–voltage ( $I$ – $V$ ) curves. The  $I$ – $V$  characteristics of a solar cell in the dark and under illumination are shown in Fig. 6.

In the dark there is almost no current flow until the start to inject at forward bias. When a cell is illuminated, the  $I$ – $V$  curve is shifted down by the short-circuit

current,  $I_{sc}$ . The maximum current that can run through the cell is determined by the  $I_{sc}$  [102].  $V_{oc}$  is related to the energetic relation between the donor and the acceptor. The energy difference between the highest occupied molecular orbital (HOMO) of the donor and the lowest unoccupied molecular orbital (LUMO) of the acceptor is closely correlated with the  $V_{oc}$  value. The solar cell operates in the fourth quadrant. At the maximum power point (MPP), the product of current and voltage is the largest. The largest power output ( $P_{max}$ ) is determined by the point where the product of voltage and current is maximized. Division of  $P_{max}$  by the product of  $I_{sc}$  and  $V_{oc}$  yields the fill factor, FF.

The photovoltaic PCE of a solar cell is determined by the following formula:

$$\eta_e = \frac{V_{oc} * I_{sc} * FF}{P_{in}} \quad (1)$$

$$FF = \frac{I_{mpp} * V_{mpp}}{I_{sc} * V_{oc}} \quad (2)$$

where  $V_{oc}$  is the open-circuit voltage,  $I_{sc}$  is the short-circuit current, FF is the fill factor and  $P_{in}$  is the incident light intensity.

The light intensity at  $1,000 \text{ W/m}^2$  with a spectral intensity distribution matching that of the sun on the earth's surface at an incident angle of  $48.2^\circ$ , which is called the AM1.5G spectrum is accepted as standard for solar cell testing [104].

An experimentally accessible value is the external quantum efficiency or incident photon to current efficiency (IPCE). IPCE is defined as the number of photogenerated charge carriers contributing to the photocurrent per incident photon [102]. IPCE is calculated using the following formula:

$$IPCE = \frac{1240 * I_{sc}}{\lambda * P_{in}} \quad (3)$$

where  $\lambda$  (nm) is the incident photon wavelength,  $I_{sc}$  ( $\mu\text{A/cm}^2$ ) is the photocurrent of the device and  $P_{in}$  ( $\text{W/m}^2$ ) is the incident power.

#### 2.4.1 Power Conversion Efficiency Reports on Organic Solar Cells

Organic solar cell research has grown rapidly during the last decades and now it is close to the level of the commercial applications. It became crucial [103] to accurately determine the efficiency values to enable a fair comparison of the results from several groups for the healthy development of this technology. Since the PCE is the representative parameter to evaluate the performance of a PV cell, the measurement of this value should be accurately determined and reported and also should be reproducible to be able to compare different devices [105].

The performance of PV cells is commonly described in terms of their efficiencies with respect to the standard reporting conditions (SRC) defined by the temperature, spectral irradiance, and total irradiance [105, 106]. The SRC for the

performance of the PV cells are as follows: 1,000 W/m<sup>2</sup> irradiance, AM 1.5 global reference spectrum, and 25°C cell temperature.

Shrotriya et al. have already described what must be done for accurate measurement and characterization of organic solar cells [105]. They performed experiments on polymer/fullerene bulk heterojunction solar cells and small organic molecule-based bilayer cells. They considered the effects of the spectral-responsivity, light source calibration and spectral mismatch factor and also the device area. They first investigated the effect of the light bias intensity on the spectral responsivity. They observed that the responsivities of all the cells show a slight dependence on the light bias intensity, although the behavior was different for different material systems. However, they showed that the light bias dependence of the responsivity for all test cells was constant with respect to the wavelength, which suggested that the mismatch factor calculation would be independent of light bias intensity. They also observed relatively weak dependence of the external quantum efficiency on light bias intensity. They counted the response of the cell to the chopped light as an important factor that has to be considered when measuring the spectral response of the PV device.

A solar simulator replicates the solar spectrum and is used for testing PV devices. Reference cells are used to set the intensity of a light source to a particular test condition (e.g., one sun) for *I-V* measurements. The relative spectral responsivities of the test and reference cells are an important factor in the solar simulator calibration procedure. For crystalline solar cells, the reference cell is made of the same materials and technology as the test device. The primary interest in a reference cell is the stability in the reference cell's calibration value. For this reason most thin-film organic and inorganic devices use a Si reference cell that may have a filter to improve the spectral match. However, for polymer and small organic molecule organic solar cells, it is extremely difficult to fabricate reference cell from the same materials. The reasons for this are the lack of the consistent reproducibility and the poor life times of these devices. Therefore, for the purpose of light source calibration for organic solar cell testing, it is important to select a reference cell whose spectral response matches that of the actual test cells as closely as possible to minimize the spectral error [105].

Another parameter to consider is the lamp's age, which affects the actual irradiance. As a result, the spectral mismatch changes with the age of the solar simulator's lamp. The spectral mismatch factor accounts for deviations in the spectral output of the solar simulator with respect to the standard AM1.5G spectrum and deviations in the spectral response with respect to that of the reference cell [10, 107].

It is also essential to correctly measure the device area in order to accurately determine the current density through the device. Usually, device area is chosen as the area defined by the shadow mask used for evaporating the top contact. An important factor that can result in significant errors in the estimation of the area is the shadow effect arising from evaporating successive layers from multiple sources [105].



**Fig. 7** Two common layouts for OPV devices with unpatterned PEDOT:PSS (Baytron) and photoactive layers: **a** In devices with the crosses layout, the Al electrode overlaps with the photoactive and PEDOT:PSS layers outside the patterned ITO region, **b** in this layout, outside the nominal area, the photoactive layer is in contact with unpatterned PEDOT:PSS/ITO only. Reproduced with permission from Cravino et al. [108], Copyright Wiley-VCH Verlag GmbH&Co. KGaA

Besides device area, device design can also affect the determination of the efficiency of organic solar cells. Cravino et al. demonstrated that the shape and size of a cell, which is referred to as the cell layout, might be very important in organic solar cells (see Fig. 7) [108]. They investigated the two common layouts for organic solar cells with patterned PEDOT:PSS layers and photoactive layers, as shown in the Fig. 7. They considered the results of the geometrically resolved photocurrent measurements and concluded that the most critical region in the crossed layout is the region where the Al electrode overlaps with the both photoactive and PEDOT:PSS layers.

The relationship between the performance and the electrode geometry of organic solar cells was also investigated by Kim et al. [109]. They used the two most commonly used electrode geometries: (i) island-type and (ii) crossbar-type, as shown in the figure. They found that the commonly used PV cells can produce a significant error in PCE measurement if the beam diameter of the illuminated light is larger than the area of electrodes. They concluded that the larger PCE observed using such a configuration is due to the excess photocurrent generated from a parasitic organic solar cell structure, where the conductive PEDOT:PSS layer acts as an effective anode. This can also explain why the excess photocurrent is proportional to the conductivity of the PEDOT:PSS layer and increases with the illuminated area. Kim et al. suggested two solutions to prevent the error in characterization: (i) making the area of light illumination equal to that of the active electrode of the PV cells and (ii) island-type cathode design. Considering the technical difficulty of the former method they suggested that the latter approach would be more convenient and practical (see Figs. 8 and 9) [109].

There are also other challenges in PCE measurements since there are many other parameters such as processing conditions [14, 16, 110, 111], solvent selection [10], and the presence of oxygen and moisture [50, 112], which will be discussed later.

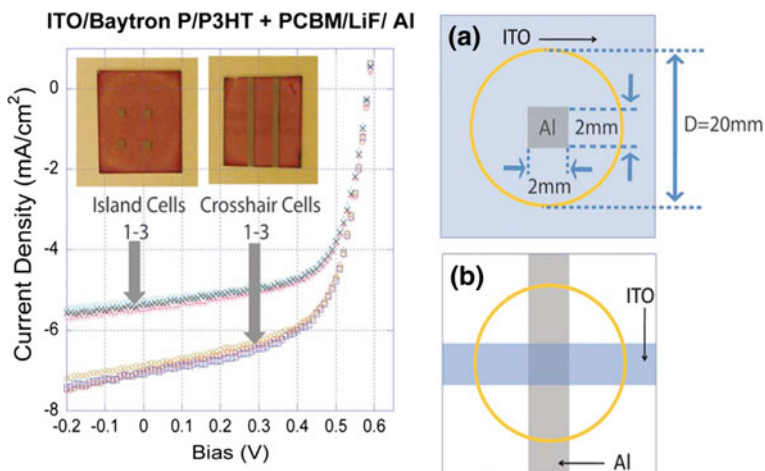


**Fig. 8**  $I$ - $V$  curves of OPV cells having (a) island-type electrode geometry and (b) crossbar-type electrode geometry \_illumination diameter: 20 mm, intensity: AM1.5G 100 mW/cm<sup>2</sup>. For the device characterization having the island-type electrode, the anode contact was made using a probe and the cathode contact was made using a gold wire. Reprinted with permission from Kim et al. [109] Copyright (2008), American Institute of Physics

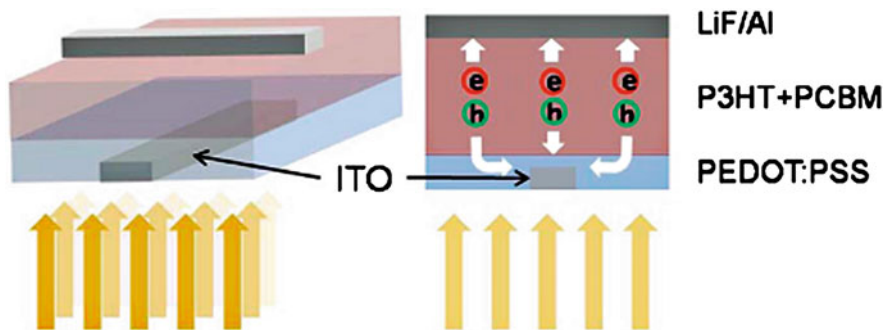


**Fig. 9** *Left* Characterization scheme of OPV cells having crossbar-type electrode geometry under illumination larger than the overlapped area of the crossbar-type electrodes. *Right* Excess current generation in PEDOT:PSS/Al device where there is no ITO. Reprinted with permission from Kim et al. [109]. Copyright (2008), American Institute of Physics

## 2.5 Characteristic Parameters of an Organic Solar Cell

### 2.5.1 Open-Circuit Voltage

One of the key parameters of PV devices is the open-circuit voltage ( $V_{oc}$ ), which is the voltage for which the current in the external circuit equals to zero [113]. Since the efficiency of an organic solar cell is directly proportional to the  $V_{oc}$ ,

improvement of the  $V_{oc}$  is crucial to achieve higher efficiencies. However, there is a controversial debate in the literature on the nature of the  $V_{oc}$ .

A generally accepted estimate for the built-in potential is given by the  $V_{oc}$ , which underestimates the built-in potential at room temperature and converges to the correct value at low temperatures [98, 106]. In a MIM device the  $V_{oc}$  is determined by the difference in the work functions of two metal contacts [84].

The PV effect in diode structures formed with thin films of PPV sandwiched between ITO and either aluminium (Al), magnesium (Mg) or calcium (Ca) was studied by Marks et al. [107]. Under illumination incident through the ITO contact, they measured large open-circuit voltages. They compared the difference in the work function between ITO and the metal in question by taking a value for the ITO work function of 4.8 eV. They found that the measured photovoltages for Mg and Ca devices approximately scaled with the metal work function, whereas the photovoltage measured in Al devices was larger than expected from the work function difference of the contact materials. Although the situation was unclear, they commented that the surface layer of the Al reacts with PPV to form covalent bonds across the vinylene linkages and introduces a non-conjugated barrier layer [107].

The magnitude of  $V_{oc}$  can be attributed to the electrode work function difference [108]. However, other research studies showed that there are other parameters that contribute to the  $V_{oc}$ , such as dark currents [114], Fermi level pinning [91] and chemical potential gradients [115, 116].

A scaling of the open-circuit voltage with electrode work function difference has also been observed in bilayer devices by Ramsdale et al. [116]. However, they observed an additional intensity-dependent contribution from the active layer within the device. This additional contribution was attributed to photoinduced generation of carriers.

Built-in potential is an essential parameter of PV devices and influences charge dissociation, charge transport, and charge collection [98]. Compared to devices made from pristine conjugated polymers, the nature of the thin-film devices made by mixing fullerenes and conjugated polymers is completely modified and, thus, the  $V_{oc}$  of the corresponding cells differ. Therefore, the MIM model or the Schottky junctions [117, 118] that successfully explain the situation in pristine polymer-based devices cannot satisfactorily explain the nature of  $V_{oc}$  in BHJ solar cells [98].

Brabec et al. investigated the critical parameters influencing the built-in potential in conjugated polymer/fullerene based devices. They analyzed the open-circuit voltage of the corresponding devices as a function of the acceptor strength [98]. They observed that the  $V_{oc}$  of the corresponding devices correlated directly with the acceptor strength of the fullerenes, whereas it was rather insensitive to variations of the work function of the negative electrode. They discussed their observations within the concept of Fermi level pinning between fullerenes and metals via surface charges.

Gadisa et al. measured and compared  $V_{oc}$  of solar cells based on series of conjugated polythiophene polymers. In every cell, they blended donor polymer with an electron acceptor fullerene molecule. They constructed devices in a sandwich structure with ITO/metallic polymer (PEDOT:PSS) acting as the anode



and Al or LiF/Al acting as a cathode. Comparing the  $V_{oc}$  of all the cells they showed that this important PV parameter systematically varied with the polymer. The variation of photovoltage was attributed to the variation of the oxidation potential of the donor conjugated polymers after due consideration of the different injection conditions in the varying polymers [119].

The influence of an altered doping level of the hole collecting electrode was investigated by Frohne et al. [73] and they observed that the  $V_{oc}$  can be influenced by the electrochemical potential of the PEDOT:PSS.

The morphology of the active layer in BHJ solar cells also affect the  $V_{oc}$ . Liu et al. introduced a new term, which is the product of cross-sectional area physically occupied by  $C_{60}$  ( $c$ ) that is related to the concentration of  $C_{60}$  in the composite and the product of  $f$ , which is the morphology induced interfacial factor and they concluded that the observed  $V_{oc}$ 's can be used to estimate  $cf$  for PV devices fabricated with different solvent [120].

The  $V_{oc}$ 's of BHJ solar cells based on PCBM as the electron acceptor and poly[2-methoxy-5(3',7'-dimethyloctyloxy)-*p*-phenylene vinylene] ( $OC_1C_{10}$ -PPV) as the electron donor were investigated by Mihailetchi et al. [97]. They demonstrated that for non-ohmic contacts, the experimental  $V_{oc}$  was determined by the work function difference of the electrodes. A total variation of more than 0.5 V of the  $V_{oc}$  was observed by variation of the negative electrode (cathode) work function. They added that for ohmic contacts the  $V_{oc}$  was governed by the LUMO and HOMO levels of the acceptor and donor, respectively, which pin the Fermi levels of the cathode and anode. According to this work, the band bending created by accumulated charges at the ohmic contact produced considerable loss in  $V_{oc}$  of 0.2 V at room temperature. They concluded that the experimentally observed voltage loss in  $V_{oc}$  of 0.38 V due to the presence of ohmic contacts at both interfaces strongly limited the maximum open-circuit voltage of  $OC_1C_{10}$ -PPV/PCBM solar cells [97].

In another study, by Mihailetchi et al., they observed that an increase in the workfunction of the metal top electrode led to a reduction of the open-circuit voltage, short-circuit current, and PVE of organic bulk-heterojunction solar cells. They demonstrated that the photocurrent obtained from an active layer comprised of a blend of  $OC_1C_{10}$ -PPV and PCBM, with lithium fluoride-topped aluminum, silver, gold, or palladium electrodes, showed a universal behavior when scaled against the effective voltage across the device. Model calculations confirmed that the dependence of the photocurrent on the effective voltage was responsible for the observed variation in performance of each different electrode. Consequently, for any given metal, only the device's open-circuit voltage was required in order to be able to predict the remaining solar cell parameters [99].

Koster et al. investigated the  $V_{oc}$  of polymer:fullerene BHJ solar cells as a function of light intensity at different temperatures [113]. The devices consisted of PPV derivative as the hole conductor and PCBM as the electron conductor. The observed photogenerated current and  $V_{oc}$  varied with classical *p-n* junction based models. They showed that the  $V_{oc}$ , when plotted as a function of light intensity, had a slope equal to  $kT/q$ . They explained the influence of light intensity and

recombination strength on  $V_{oc}$  by a model based on the notion that the quasi-Fermi levels were constant throughout the device, including both drift and diffusion of charge carriers.

Scharber et al. investigated the relation between the energy levels of the donor-acceptor blend and the  $V_{oc}$  of 26 different BHJ devices [30]. They derived a simple relation between the energy level of the HOMO of the polymer and the  $V_{oc}$ , which was used to estimate the maximum efficiency of BHJ solar cells. Based on the model, they determined the ideal material parameters for a conjugated polymer-PCBM device. They demonstrated that for a total of 26 different BHJ solar cells, there was a linear relation between  $V_{oc}$  and the conjugated polymer oxidation potential. They estimated the  $V_{oc}$  of a conjugated polymer-PCBM solar cell using the following formula [30]:

$$V_{oc} = (1/e)(|E^{\text{DonorHOMO}}| - |E^{\text{PCBMLUMO}}|) - 0.3 \text{ V} \quad (4)$$

where  $e$  is the elementary charge and using  $-4.3$  eV for the PCBM LUMO energy. The value of  $0.3$  V in Eq. 4 is an empirical factor. They found that the MIM model is not applicable to BHJ devices. The observed deviation of  $V_{oc}$  from  $V_{BI}$  (HOMO donor minus LUMO of the acceptor), which they related to the working principle of the BHJ and they suggested that it could be minimized by optimizing materials, the active layer thickness, and the charge carrier mobility [30].

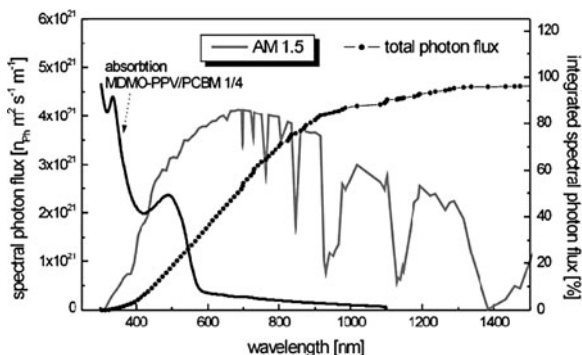
### 2.5.2 Short Circuit Current

Since  $I_{sc}$  also directly affects the efficiency, it is an essential parameter of the solar cells. Theoretical calculations predict that the development of novel donor materials is required to reach efficiencies of 10% or more [30]. New materials should also be considered to overcome the limitations of MDMO-PPV/PCBM or P3HT/PCBM-based devices. One important problem is limited absorption. It was calculated that 240 nm-thick P3HT is only capable of absorbing 21% of the sun's photons [121] and only in the wavelength range between 350 and 650 nm. Conjugated polymers have absorption coefficients in the order of  $10^5 \text{ cm}^{-1}$  [122]. The limitation in the absorption is due to the mismatch of the absorption of the organic semiconductor and the solar spectrum (see Fig. 10).

A polymer having a 1.1 eV band gap can absorb 77% of all the solar irradiation. However, majority of semiconducting polymers have band gaps higher than 2 eV, which limits the possible absorption [122]. This limitation led researchers to investigate low band gap polymers, which are achieved by shifting the polymer absorption spectrum into the near-infrared region.

The synthesis and application of low band gap polymers that absorb light above 600 nm in organic solar cells have been reported by several groups [124–130]. The band gap is defined as the difference between the HOMO and LUMO energy levels in polymers, neglecting Coulombic interactions. Low band gap polymers are defined as those having band gaps below approximately 2 eV [131]. One of the

**Fig. 10** AM1.5G spectrum compared to the absorption profile of a MDMO-PPV:PCBM (1:4) film. Circles show the total photon flux, i.e., the percentage of photons available for a material with a certain bandgap. Winder and Sariciftci [123] Reproduced by permission of the Royal Society of Chemistry (<http://dx.doi.org/10.1039/B306630D>)



limiting parameters in plastic solar cells is the mismatch of the absorption of organic materials and the terrestrial solar spectrum [130]. The optical band gap of the generally used CPs in organic solar cells have values around 2.0–2.2 eV [130]. The use of low band gap polymers expands the spectral region of bulk heterojunction solar cells and is a viable route to enhance the number of photons absorbed [130]. An ideal band gap of 1.3–1.6 eV for a bulk heterojunction device is described in a study by Scharber et al. [30].

Another way to overcome the barrier to absorbing more photons is increasing the layer thicknesses. However, one should note that an increase in the layer thickness may be limited by the charge carrier mobility and lifetime. At present, bulk heterojunction polymer solar cells are typically fabricated with an active layer thickness of between 80 and 100 nm. This active layer thickness has traditionally been chosen based on convenience and empirical results. However, it was studied by Moule et al. that active layer thickness has an effect on the short-circuit current and efficiency of BHJ polymer solar cells [132]. They demonstrated that the performance of these devices was highly dependent on the active layer thickness and, using a model for optical interference, they showed that such effects were responsible for the variations in performance as a function of active layer thickness. They also showed that the ideal composition ratio of the donor and acceptor materials was not constant, but depended on the active layer thickness in a predictable manner. Also, they confirmed that their results are not material specific and that high efficiency solar cells can be fabricated with active layer thickness greater than 100 nm [132].

The optical properties of BHJ solar cells were modelled by Hoppe et al. [133]. They showed that upon illumination of BHJ solar cells using MDMO:PPV/PCBM with the standard AM1.5G solar spectrum, the short-circuit current can be determined for any given internal quantum efficiency as a function of the active layer

thickness. Also, the depth profile of photoinduced charge-generation rates were calculated.

Peumans et al. demonstrated a method for efficient photon harvesting in organic thin films, thereby increasing the efficiency of organic PV cells [134]. By incorporating an EBL between the photoactive organic layers and the metal cathode, they achieved an external PVC of  $2.4\% \pm 0.3\%$  from vacuum-deposited ultrathin organic bilayer PV cells employed in a simple light trapping geometry.

As mentioned above, the optical absorptions of conjugated polymers are strong, but even at maximum absorption, the penetration depth of light into these materials is in the range of 10–100 nm [135]. Therefore, the generation of excited states over 10–100 nm deep and harvesting, which occurs over a much shorter distance, must be combined. Making thicker films to collect more light by absorption decreases the field and reduces the collection efficiency. One way of bringing these requirements together is to trap light in the polymer layers by diffraction into guided modes in the thin polymer films [135]. This approach has been used to enhance light trapping and absorption in silicon solar cells in the energy range where optical absorption range in silicon is low [136]. Since optical absorption in conjugated polymers is high, Roman et al. used a similar approach to trap light in thinner polymer films [135]. They used an elastomeric mold to transfer a submicron grating pattern from a commercially available grating template to the active polymer layer in a PV device. They concluded that the grating function improved the optoelectronic properties of photodiodes [135].

Niggemann et al. also investigated two novel cell concepts: light trapping with diffraction gratings and buried nano electrodes [137]. In the buried electrode approach, they used one planar electrode and the other electrode was oriented perpendicular to the substrate surface, forming a lamellar structure. In this case low mobility charge carriers could be collected at the lamellar electrodes and high mobility charge carriers could be collected at the planar electrode. In their study, they discussed the potential of this approach and the initial experimental results [137].

### 2.5.3 Fill Factor

The fill factor of a device depends on charge dissociation, charge carrier transport, and recombination [138]. Effective cell design variables have large impact on the FF of an OPV device. The characteristic properties of an organic layer such as morphology and thickness, the regioregularity of the conjugated polymer, and the two interfaces between the electrodes and the blend layer have a large impact on the FF by affecting the series resistance ( $R_s$ ), and the shunt resistance ( $R_{sh}$ ). The  $R_s$  can be calculated from the inverse slope of the  $I$ - $V$  curve in the first quadrant and is closely correlated with the intrinsic resistance, morphology, and thickness of the semiconductor layer whereas the  $R_{sh}$  is correlated with the amount and character of the impurities and defects in the active organic semiconductor layer since impurities and defects cause charge recombination and leakage current, as described by

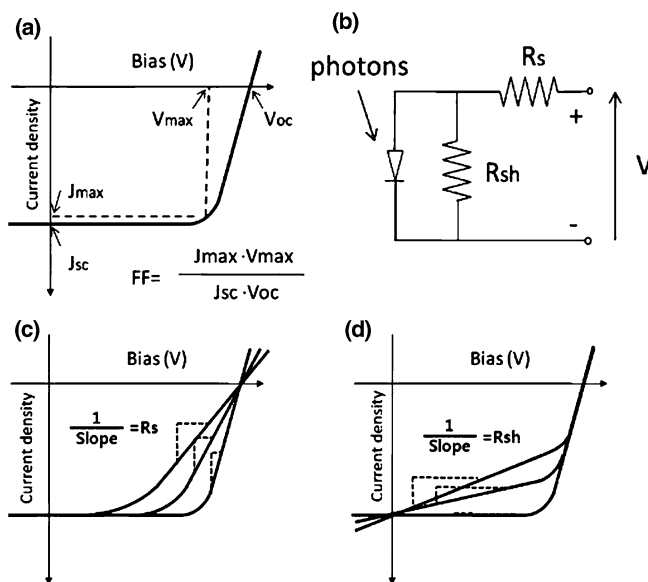


**Fig. 11** **a** Definition of FF.  $J_{\max}$  is the current density at the maximum of  $JV$  in the fourth quadrant and  $V_{\max}$  is the bias at the maximum of  $JV$  in the fourth quadrant. **b** Circuit model of a photovoltaic device.  $R_s$  is the series resistance and  $R_{sh}$  is the shunt resistance. **c** Impact of the variation of the series resistance ( $R_s$ ) on the FF. The indicated inverse slope represents  $R_s$ . **d** Impact of the variation of the shunt resistance ( $R_{sh}$ ) on the FF. The indicated inverse slope represents  $R_{sh}$ . Reprinted with permission from Kim et al. [139]. Copyright (2009), American Chemical Society

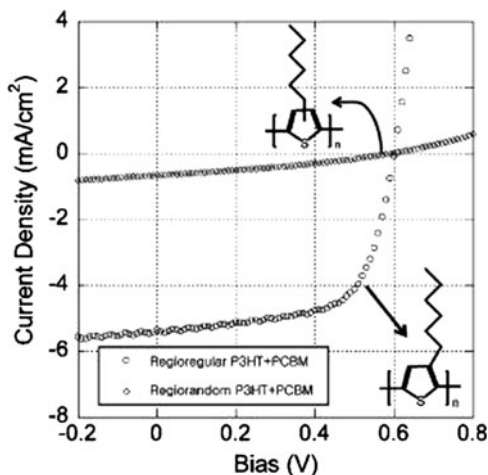
Kim et al. [139] (see Fig. 11).  $R_{sh}$  determines the inverse slope of the  $I-V$  curve in the fourth quadrant.

The FF is determined using Eq. 2, which is basically the ratio of the product of maximum voltage and maximum current defined by the MPP and the product of the  $V_{oc}$  and  $I_{sc}$ .

Gupta et al. studied the fill factor in organic solar cells and observed that the shape of the  $I-V$  characteristics in the power generating fourth quadrant strongly depends on the quality of polymer-cathode interface and does not always reflect the bulk characteristics [138]. They pointed out that a partial metal coverage or a chemically modified layer can reduce the FF drastically. They concluded that defects at the polymer-metal interface give rise to charge carrier accumulation due to inefficient collection. They suggested that a conformal coating of metal that follows the polymer surface undulations is a preferable way to improve the FF [138].

Effective variables to control the FF of organic solar cells were studied by Kim et al. [139]. They reported relationships between the FF and various design parameters. Their device structure was ITO/PEDOT:PSS/P3HT+PCBM/LiF/Al.

**Fig. 12** Effect of regioregularity of conjugated polymers on the fill factor. Reprinted with permission from Kim et al. [139], Copyright (2009), American Chemical Society



They used the island-type electrode geometry to prevent additional charge collection observed in the crossbar-type device configuration, as described in Ref. [109]. They investigated the effects of characteristic properties of the organic layer to the FF, including morphology, thickness, the regioregularity of the conjugated polymer, and the two interfaces between the electrodes and the blend layer [139]. Their results showed that when the crystallinity of the blend layer was increased by thermal annealing,  $R_s$  decreased. When the regioregular P3HT was investigated, they observed that  $R_s$  was also reduced by one order of magnitude. They pointed out that the higher crystallinity induced by thermal annealing and regioregularity enhance the efficiency of the inter- and intramolecular charge transport [139] (see Fig. 12).

They observed that as the thickness of the blend layer was increased,  $R_s$  increased and  $R_{sh}$  decreased, which they attributed to the increased distance the charges must travel until they reach the electrodes, possibly increasing the resistivity and charge recombination (see Fig. 13).

They also studied the quality of two interfaces between the blend layer and the electrodes. They found that when a less conducting cathode was used, the FF decreased because of more charge recombination and leakage current, which was confirmed by the decrease in  $R_{sh}$  [139] (see Fig. 14).

They also proved that  $R_{sh}$  and the resulting FF were largely affected by the efficiency of charge extraction through the cathode, which they investigated by controlling the amount of the photoinduced charges in the blend layer through various illumination conditions. They observed that as the illumination intensity increased,  $R_{sh}$  and FF gradually decreased, indicating that there is more charge recombination in the blend layer. Finally, they showed that the nature of the interface between the Al anode and the blend layer also impacts the FF [139].

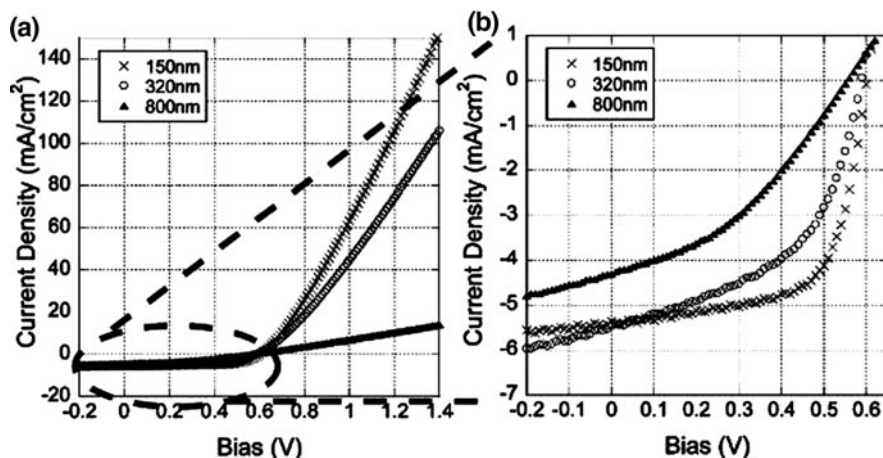


Fig. 13 Thickness effect on the fill factor. Reprinted with permission from Kim et al. [139]. Copyright (2009), American Chemical Society

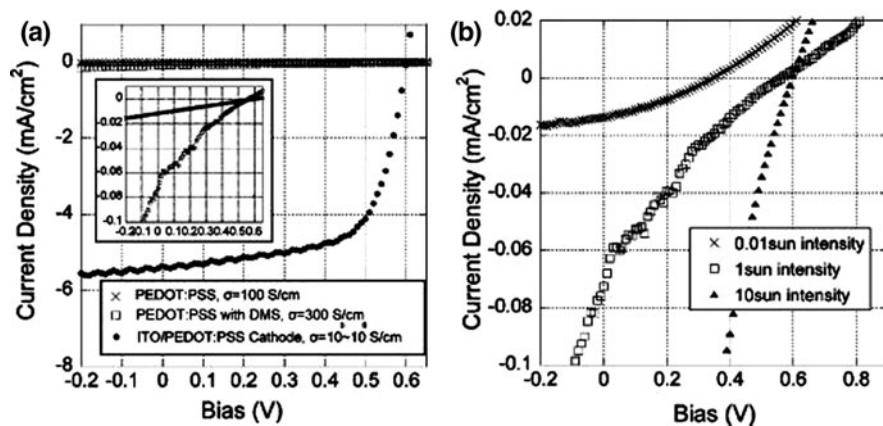


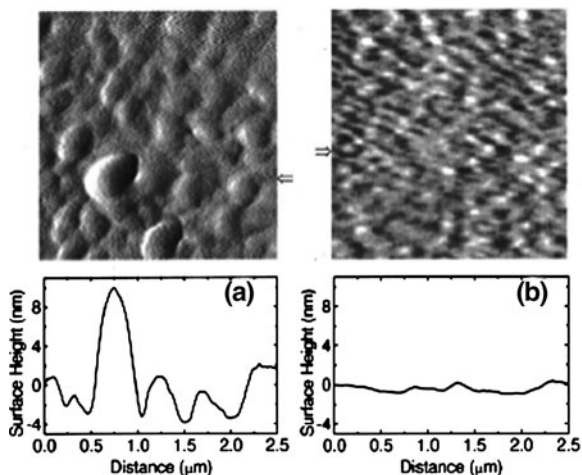
Fig. 14 a Effect of anode conductivity, b effect of illumination intensity on the fill factor. Reprinted with permission from Kim et al. [139]. Copyright (2009), American Chemical Society

### 3 Nanomorphology and Charge Transport in Organic Solar Cells

#### 3.1 Nanomorphology

The BHJ concept requires blending two organic materials, one of which is a donor (generally a conjugated polymer) and the other is an acceptor (generally a fullerene derivative). Even if these donors and acceptors have an ideal electronic

**Fig. 15** AFM images showing the surface morphology of MDMO-PPV:PCBM (1:4 by wt) blend films with a thickness of approximately 100 nm and the corresponding cross-sections. **a** Film spin coated from a toluene solution. **b** Film spin coated from a chlorobenzene solution. Reprinted with permission from Shaheen et al. [10]. Copyright (2001), American Institute of Physics



relationship, the performances of BHJ solar cells depend on the physical interaction of the donor and acceptor components, which is evidenced by the composite morphology. The ideal bulk heterojunction solar cell is defined as a bicontinuous network of donor and acceptor materials with a maximum interfacial area for exciton dissociation and a domain size proportional to the exciton diffusion length [9]. The morphology of the active layer depends on the properties of the polymer and the fullerene, such as interaction between two components (miscibility), and on influences associated with the device fabrication, such as the choice of the solvent, concentration of the polymer-fullerene components, deposition technique, and thermal annealing [140].

The PCE of OPV devices based on conjugated polymer/methanofullerene blends are dramatically affected by the molecular morphology [10] (see Fig. 15). Shaheen et al. reported one of the earliest studies [10]. They fabricated a device with a PVC of 2.5% under AM1.5G illumination by structuring the blend to be a more intimate mixture that contains less phase segregation of methanofullerenes, simultaneously increasing the degree of interactions between conjugated polymer chains. They showed that the choice of the proper casting solvent may lead to high PCEs. Shaheen et al. fabricated devices using MDMO:PPV and PCBM. Figure 15 shows the atomic force microscopy (AFM) images of the surfaces of MDMO-PPV:PCBM blend films spin coated using either toluene or chlorobenzene.

Measurement of the mechanical stiffness and adhesion properties of the surface indicated that the vertical features on the AFM images have a chemical composition different than the surrounding valleys. Since these features were not observed in pristine films of MDMO-PPV, they assigned them to be phase-segregated regions that contain a different fullerene concentration. In the case of chlorobenzene as the solvent they observed much more uniform mixing of the constituents. Their results indicated that spin coating the active layer blend from



chlorobenzene has the effect of simultaneously enhancing the morphological microstructures of both components that form the interpenetrating networks [10].

The conformation of the polymer chains can be controlled by the selection of the organic solvents, by the concentration of the polymer solution, and by the rotational speed of the spin-casting process. The resulting morphology in the thin film plays an important role in controlling both the material and the device characteristics [120]. Liu et al. fabricated OPV devices by blending the conjugated polymer, poly (2-methoxy-5-(2'-ethylhexyloxy)-1,4-phenylenevinylene) (M3EH-PPV) with the buckminsterfullerene, C<sub>60</sub> [120]. They showed that the photocurrent and  $V_{oc}$  show a strong dependence on the polymer processing conditions. They found that the PV devices fabricated with tetrahydrofuran (THF) or chloroform (non-aromatic solvents) have smaller photocurrents under the same reverse bias as well as higher open-circuit voltages than the devices fabricated with xylene, dichlorobenzene, or chlorobenzene (aromatic solvents). The device performance dependence on the processing solvent was attributed to the different solvation induced polymer morphology [120].

The combination of AFM, scanning electron microscopy (SEM), and transmission electron microscopy (TEM) were applied to MDMO-PPV/PCBM blends to investigate the nanomorphology of chlorobenzene and toluene cast blends [95, 96, 100].

Van Duren et al. used a technique to resolve the morphology of spin cast films of MDMO-PPV:PCBM blends in three dimensions on a nanometer scale and related the results to the performance of the corresponding solar cells [95]. They employed AFM, TEM, and depth profiling using dynamic time of flight secondary ion mass spectrometry (TOF-SIMS) techniques. They showed that phase separation is not observed up to 50 wt% PCBM and nanoscale phase separation sets in for concentrations of more than 67 wt% PCBM. They observed that the performance of the corresponding PV devices features a strong increase in PCE when the phase separated network develops, with sharp increases in photocurrent and fill factor between 50 and 67 wt% PCBM. They concluded that as the phase separation sets in, enhanced electron transport and a reduction of bimolecular charge recombination provide the conditions for improved performance [95].

Martens et al. also observed phase separation in MDMO-PPV:PCBM based organic solar cells using both TEM and AFM. They observed a two-phase system that consists of PCBM-rich domains embedded in a matrix consisting of MDMO-PPV and PCBM. They showed that changing the solvent influences the size of the phase-separated PCBM-rich domains. They also showed that the composition of the matrix is determined by the choice of the solvent. They studied this effect by changing the ratio of PCBM relative to MDMO-PPV [96].

The relation between nanoscale morphology and the associated device properties in conjugated polymer/fullerene bulk heterojunction solar cells was also investigated by Hoppe et al. [100]. They performed measurements on devices based on blends of MDMO-PPV and PCBM, spin cast either from toluene or chlorobenzene solutions. They applied SEM and AFM techniques to characterize the nanoscale morphology. In addition, they manipulated the morphology via

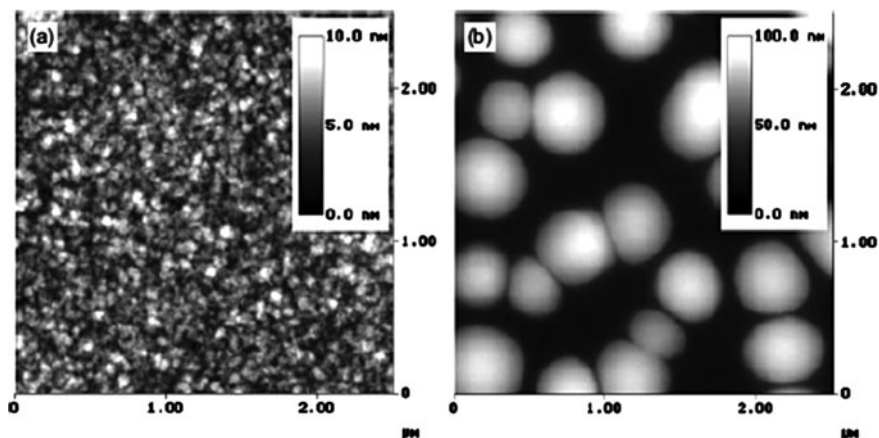


**Fig. 16** AFM topography scans of MDMO-PPV/PCBM 1:4 (by weight) blended films spin cast from (a) chlorobenzene, and (b) toluene solution. The toluene cast films shows a ten-fold greater height variation compared to the chlorobenzene cast one. Features of a few hundred nanometers in width are visible in (b), while features in (a) are around 50 nm. Reproduced with permission from Hoppe et al. [100]. Copyright Wiley-VCH Verlag GmbH&Co. KGaA.

annealing, to increase the extent of phase separation in the thin film blends and to identify the distribution of materials. They confirmed the demixing of the materials under thermal treatment using photoluminescence (PL) measurements. They observed PL luminescence of PCBM clusters with sizes up to a few 100 nm which indicated a photocurrent loss in films of the coarser phase-separated blends cast from toluene. They concluded that the scale of phase separation in the toluene cast films depends strongly on the ratio of MDMO-PPV to PCBM, as well as on the total concentration of the casting solution. They also observed small beads of 20–30 nm diameter, attributed to MDMO-PPV, in blend films cast from both toluene and chlorobenzene (see Figs. 16, 17 and 18) [96].

The degree and length scale of phase separation between the donor and the acceptor phases has also an influence on the efficiency of BHJ solar cells [141]. As previously described, the common operation principle of a BHJ solar cell requires a photogenerated exciton in the donor or acceptor phase to diffuse to the phase boundary, where charge transfer takes place. These freely or bound carriers are subsequently separated and the free charges are then transported to the contacts through the percolating paths in different phases [141]. The critical length scale for the phase separation is the exciton diffusion length, which in disordered organic materials is on the order of 5 nm [141, 142].

Recently, Maturova et al. presented a model for the device performance of BHJ solar cells that takes into account the phase separated morphology [141]. It was applied to devices with MDMO-PPV:PCBM as the active material. They found that the characteristic features of the  $I$ - $V$  characteristics and their evolution with morphology can be reproduced without taking into account exciton diffusion or field dependent dissociation of electrostatically bound charge transfer states.

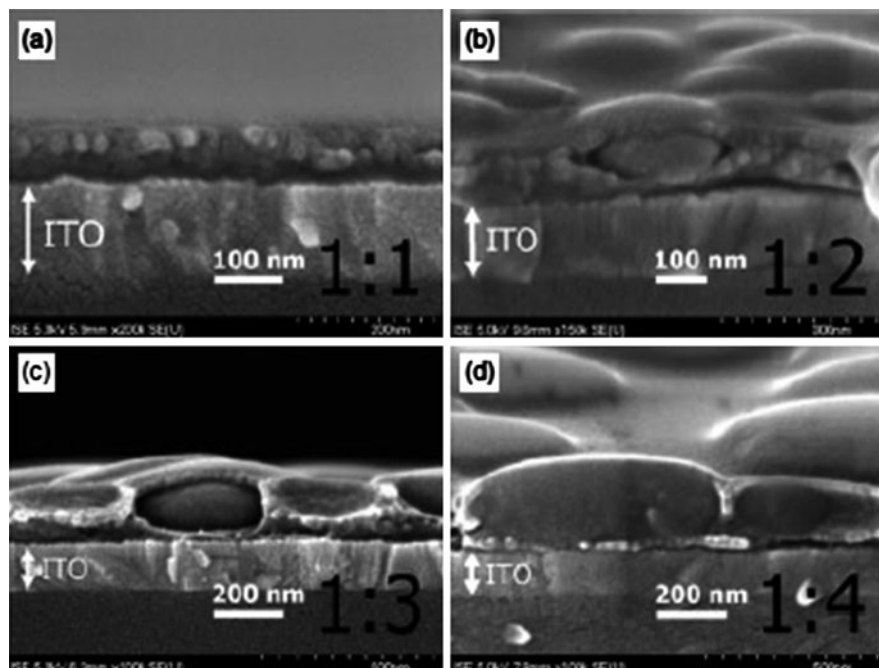


**Fig. 17** SEM side views (cross-sections) of MDMO-PPV/PCBM blend films cast from toluene with various weight ratios of MDMO-PPV and PCBM. For the ratios 1:4, 1:3 and 1:2 (**b–d**), the nanoclusters, in the form of discs, are surrounded by another phase, called the skin, that contains smaller spheres of about 20–30 nm diameter. For the 1:1 film, only these smaller spheres are found. Reproduced with permission from Hoppe et al. [100]. Copyright Wiley-VCH Verlag GmbH&Co. KGaA.

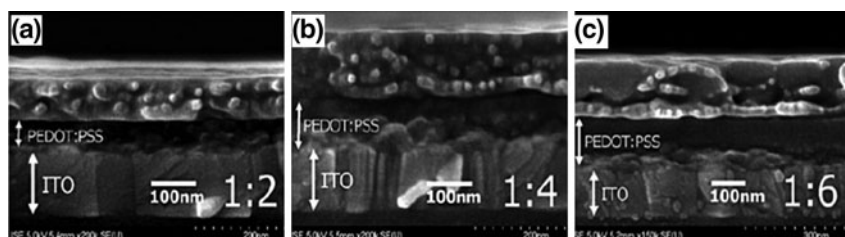


**Fig. 18** SEM side views of MDMO-PPV:PCBM blend films spin-cast from chlorobenzene solutions with various ratios (by weight) of MDMO-PPV to PCBM on top of PEDOT:PSS coated ITO glass. In all samples nanospheres of about the same size (20 nm) are found. Reproduced with permission from Hoppe et al. [100]. Copyright Wiley-VCH Verlag GmbH&Co. KGaA.

They showed that the lateral transport of free photogenerated electrons from the donor-rich to the acceptor-rich phase is the critical process. They fabricated devices by blending MDMO-PPV with PCBM and tuned the length scale of phase separation from ca 40 nm to over 500 nm by changing the solvent and varying the

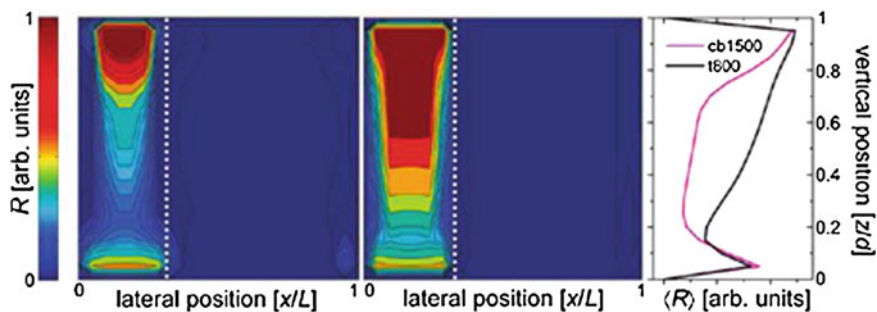


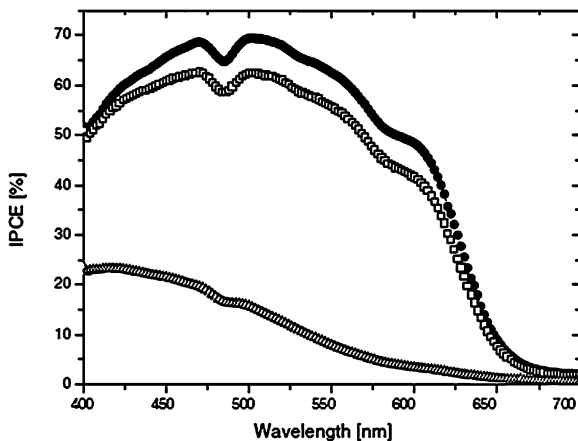
**Fig. 19** Calculated recombination rates  $R$  under short circuit conditions inside devices spin-cast from (left) chlorobenzene at 1,500 rpm and (middle) toluene at 800 rpm versus normalized vertical and lateral position. The dotted white line indicates the phase boundary. The color scale is the same for both devices. The right panel shows the averaged recombination rate for each device. Reprinted with permission from Maturova et al. [141]. Copyright (2009), American Chemical Society

spin speed. They showed that the device characteristics of polymer:PCBM BHJ solar cells are largely determined by the lateral transport of the free photogenerated electrons from the polymer-rich donor phase to the PCBM-rich acceptor phase. They pointed out that under low fields, the nanometer length scale of phase separation strongly influences the probability of escaping bimolecular recombination, leading to an increased short circuit current for finer phase separation whereas under high fields, the lateral transport is suppressed, and a transition to a vertical electron extraction pathway occurs [141] (see Fig. 19).

Regioregular P3HT (RR-P3HT) is a promising candidate for OPV research due to its stability and absorption in the red region. Currently, one of the most promising organic solar cells, both in terms of efficiency and long-term stability is the system based on regioregular P3HT as the electron donor and PCBM as the acceptor, with efficiencies of 4–5% [16, 110]. An essential step to achieve high efficiency is to subject P3HT/PCBM solar cells to an annealing treatment, either at elevated temperature or during slow solvent evaporation [143]. As a result of heating, the morphological structure of the organic active layer can be improved by reducing the free volume and the density of defects at the interface during evaporation of the solvent [15, 144] and by enhancing interchain interactions [15, 145]. It is commonly expected that morphology development in a P3HT/PCBM system depending on the film preparation method, annealing treatment should create and stabilize a nanoscale interpenetrating network with high crystalline order and favorable concentration gradients of both components through the thickness of a photoactive layer [143].

The method of thermal annealing varies in the literature. Structural, optical, and electrical properties of poly(3-dodecylthiophene) (P3DT) have been studied after heat treatment at various temperatures by Nakazono et al. [146]. They showed the crystallinity and crystallite size of P3DT increased after heat treatment. They also found that the electrical conductivity decreased with increasing the heating

**Fig. 20** IPCE of P3HT-PCBM solar cells: as-produced solar cell (*open triangles*), annealed solar cell (*open squares*), and cell simultaneously treated by annealing and applying an external voltage (*filled circles*). Reproduced with permission from Padinger et al. [14]. Copyright Wiley-VCH Verlag GmbH & Co. KGaA.



temperature. According to the results obtained they suggested that the interchain hopping of charge carrier between neighboring  $\pi$  conjugation planes is the dominant process in conductivity and carrier mobility in P3DT [146].

Studies on thermal annealing under chloroform vapor on polythiophene copolymers indicate a strong increase in the external quantum efficiency of photogenerated charge carriers [147].

Using a tempering cycle at elevated temperatures in which an external voltage is simultaneously applied, an increase in short-circuit current density and external quantum efficiency was demonstrated [14] (see Fig. 20). Padinger et al. presumed that the enhancement in the  $V_{oc}$  and the FF of post-production treated devices compared to untreated devices results partly from the burning of the shunts, while they presumed that the increase in  $I_{sc}$  results from an increase of the charge carrier mobility [14] (see Fig. 21).

The results of the studies on the electrical and physical modifications to P3HT upon thermal annealing showed that at temperatures higher than  $100^{\circ}\text{C}$ , the content of  $\text{O}_2$  could no longer be detected due to a dedoping process, and the organic absorber became protected against deterioration [148].

The influence of nanomorphology on the PV action of polymer-fullerene composites was studied by Chirvaze et al. [15]. They analyzed the consequences of thermal annealing on ITO/PEDOT:PSS/P3HT:PCBM/Al PV devices. They realized that inspite of a considerable increase in the short-circuit current density due to heat treatment, a large amount of PCBM in the P3HT:PCBM-based devices do not automatically imply a high-energy conversion efficiency. In their experimental study, the PCBM concentration in the BHJ P3HT:PCBM composites was optimized to approximately 50%, the critical value which stems from the mutual interplay between an efficient generation of mobile charge carriers via photoinduced charge transfer and an efficient carrier transport, less affected by the recombination processes [15] (see Fig. 22).

**Fig. 21** Influence of the duration of the post-production treatment on the white light efficiency ( $800 \text{ W/m}^2$ ) for different post-production treatment methods: annealing (*dotted line*) and annealing plus external voltage (*solid line*). Reproduced with permission from Padinger et al. [14] Copyright Wiley-VCH Verlag GmbH&Co. KGaA.

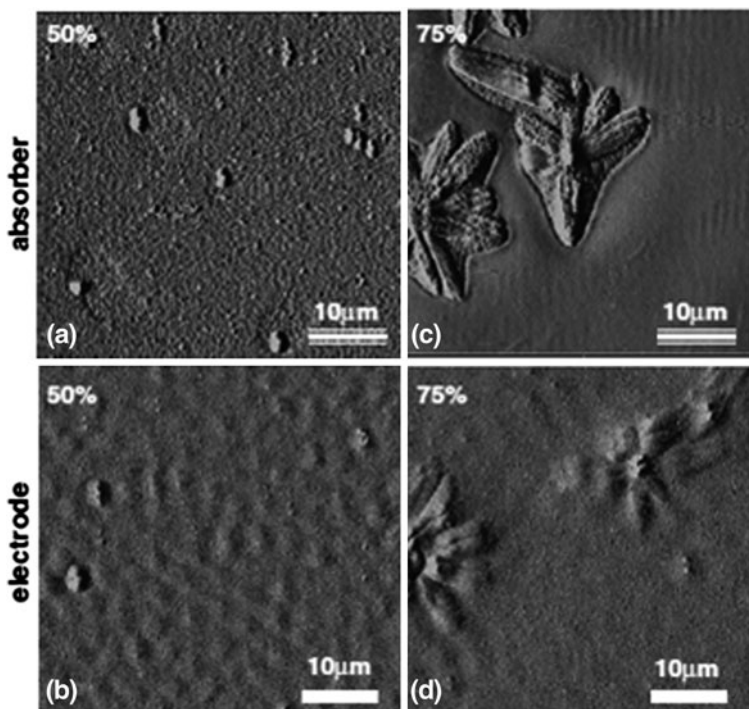
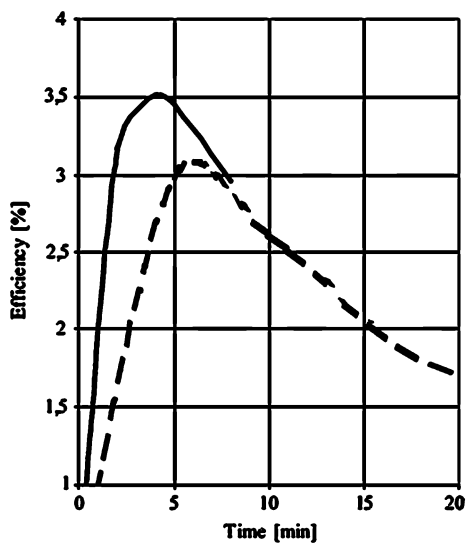


**Fig. 22** AFM images in tapping mode (phase) of the P3HT:PCBM absorber surface (**a, c**) as well as of the aluminium electrode (**b, d**) for a PCBM concentration of 5 and 75%, respectively. Scan area  $50 \times 50 \mu\text{m}^2$ . Reprinted with permission from Chirvaze et al. [15]. Copyright (2004), American Institute of Physics

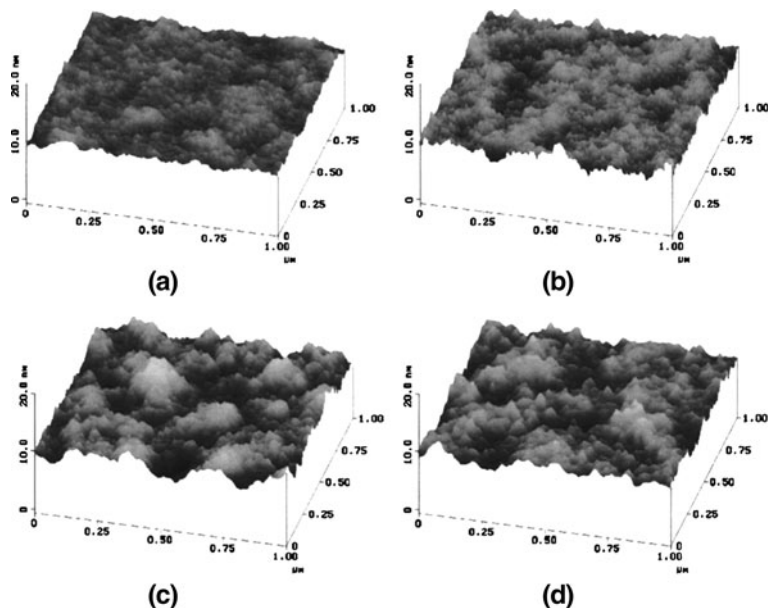


**Fig. 23** AFM height images of the surface of the active layer consisting of P3HT:PCBM with a 1:1 weight ratio **a** before annealing, and after annealing at **b** 70°C, **c** 110°C, and **d** 150°C. The annealing time for all the films was 10 min. The P3HT:PCBM films were spin-coated on top of PEDOT:PSS-coated ITO glass. Reprinted with permission from Li et al. [149]. Copyright (2005), American Institute of Physics

The effects of annealing temperature and time on the device performance for devices annealed before and after cathode deposition were studied by Li et al. [149] (see Fig. 23). They showed that thermal annealing shows significant improvement in the performance of both types of annealing conditions, with post production annealing being slightly better. They found that the best annealing condition for the device is post-production treatment at 110°C for 10 min. By keeping the optimized thermal annealing condition and varying the active layer thickness, they fabricated devices with PCEs up to 4% [149] (see Figs. 24 and 25).

The effects of solvent and annealing on the performance of P3HT:PCBM-based organic solar cells were studied by Al Ibrahim et al. [150]. They fabricated P3HT:PCBM devices using two different solvents. They showed that the P3HT:PCBM films cast from chlorobenzene solution absorbed more red light than the films cast from chloroform solution. After thermal annealing, the films cast from chloroform showed higher absorption than the films cast from chlorobenzene. They observed that solar cells made from P3HT:PCBM chlorobenzene solution showed no change in the white light PVC after annealing. They concluded that the solar cells processed from P3HT:PCBM chloroform solution showed higher PCEs after annealing [150].

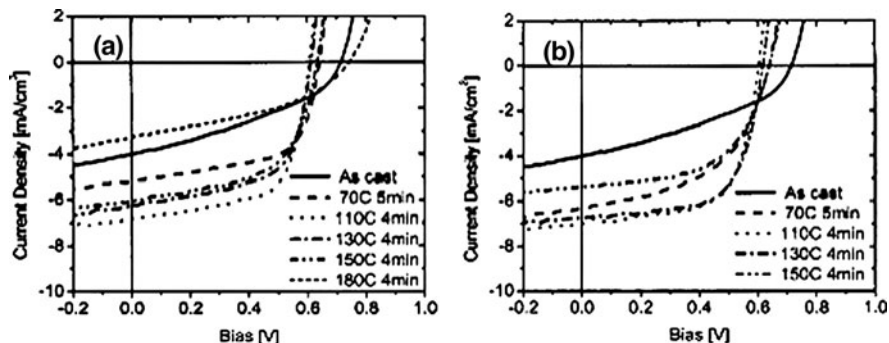


Fig. 24  $I$ - $V$  characteristics under an illumination of  $100 \text{ mW/cm}^2$  AM1.5G for devices that have undergone annealing **a** pretreatment and **b** post-production treatment. The different curves represent different annealing temperatures ranging from room temperature to  $180^\circ\text{C}$ . Reprinted with permission from Li et al. [149]. Copyright (2005), American Institute of Physics

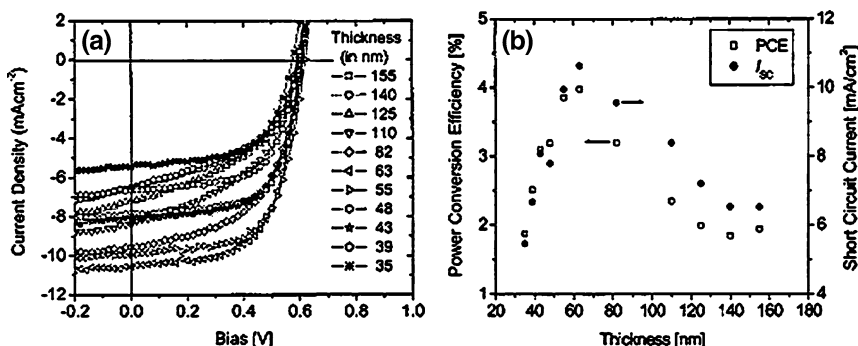


Fig. 25 **a**  $I$ - $V$  characteristics under illumination for photovoltaic device based on P3HT:PCBM with a 1:1 weight ratio and varying active layer thickness, and **b** short-circuit current density and PCE as a function of active layer thickness. All the devices here were annealed at  $110^\circ\text{C}$  for 10 min post-production. Reprinted with permission from Li et al. [149]. Copyright (2005), American Institute of Physics

Erb et al. studied the correlation between structural and optical properties of composite P3HT/PCBM films [151]. They investigated the structural properties of P3HT:PCBM films using grazing-incidence X-ray diffraction (XRD) and determined the size and orientation of crystalline P3HT nanodomains. They did not detect PCBM crystallites in thin films by XRD. Upon annealing, they observed that the P3HT crystallinity increases, leading to an increase in the optical absorption and spectral photocurrent in the low photon energy region. They demonstrated a direct relation between efficiency and P3HT crystallinity [151].

Savenije et al. investigated the influence of various thermal treatment steps in the morphology and photoconductive properties of a non-contacted, 50 nm thick



blend of P3HT and PCBM [152]. They characterized the films using TEM and electrodeless time resolved microwave conductivity (TRMC) techniques. They observed that after annealing the film for 5 min at 80°C, the TEM images showed the formation of crystalline fibrils of P3HT due to a more ordered packing of the polymer chains. They found that the thermal treatment results in a large increase of photoconductivity due to an enhancement of hole mobility in these crystalline P3HT domains from 0.0056 cm<sup>2</sup>/Vs for the non-annealed sample to 0.044 cm<sup>2</sup>/Vs for the annealed sample. They demonstrated that further annealing of the sample at 130°C results in the formation of three different substructures within the heterojunction: a PCBM:P3HT blend with PCBM-rich clusters, a region depleted of PCBM and large PCBM single crystals. A tenfold rise in decay time of the photoconductivity was explained by the authors by the formation of PCBM-rich clusters and large PCBM single crystals, resulting in an increased diffusional escape probability for mobile charge carriers and hence reduced recombination [152].

Yang et al. used TEM and electron diffraction to study the changes in morphology of P3HT:PCBM-based devices (see Fig. 26) [153]. They showed that thermal annealing produces and stabilizes a nanoscale interpenetrating network with crystalline order for both components. They demonstrated that P3HT forms long, thin conducting nanowires in a rather homogeneous, nanocrystalline PCBM film. They explained the increase in the PCE observed in these devices as a result of both the improved crystalline nature of films and increased but controlled demixing between the two constituents after annealing [153].

Van Bavel et al. performed an analysis of the three dimensional (3D) nanoscale organization of P3HT/PCBM photoactive layers before and after annealing treatments with nanometer resolution in all three dimensions by applying the technique of electron tomography (ET), with the aim to identify the critical morphology parameters contributing to the improved performance of annealed devices; they identified the critical morphology parameters contributing to the improved performance of P3HT/PCBM solar cells after thermal or solvent assisted annealing [143]. They explained that after spin-coating from solution, few aggregates of P3HT are present in the film and the overall crystallinity of P3HT is quite low. However, they showed that after annealing, reorganization of the P3HT/PCBM morphology takes place: many highly crystalline and long (up to several microns) P3HT nanorods form over the volume of the films. These nanorods form a genuine 3D network, which was proved by ET, and serve as physical barriers to PCBM diffusion by suppressing a large-scale phase separation at any point in the film preparation process. The authors concluded that all of the morphological changes in the P3HT/PCBM system after thermal or solvent assisted annealing result in improved photon absorption, better exciton dissociation, and more efficient and balanced transport of free charges to the electrodes, and are reflected in higher values of FF and  $J_{sc}$ , and hence better overall efficiency of corresponding solar cell devices (see Figs. 27 and 28) [143].

Another ET study on imaging the 3D nanostructure of a polymer cell was performed by Andersson et al. [154]. In ET, three-dimensional reconstructions are

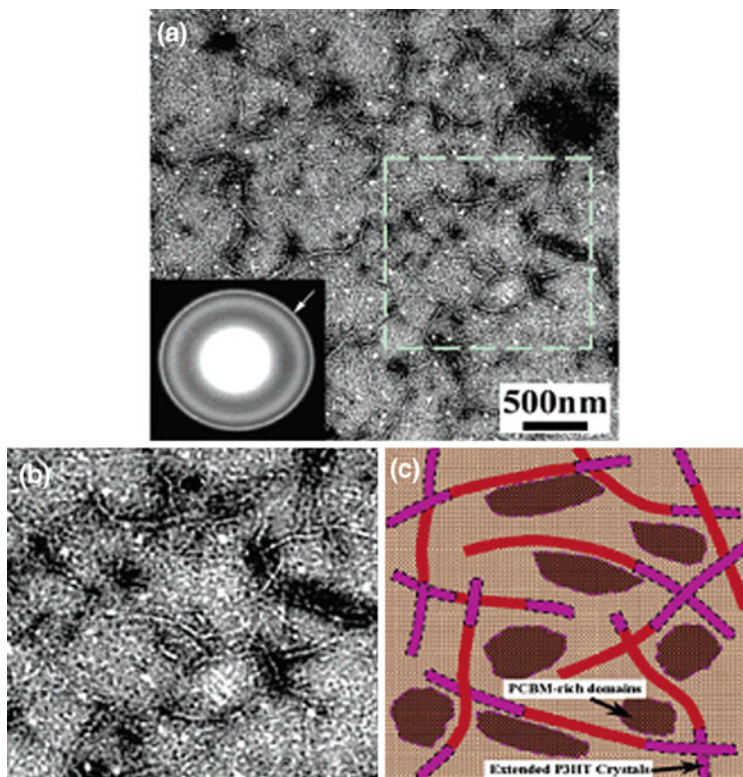


**Fig. 26** BF TEM images show the overview (a), the zoom-in (b) and the corresponding schematic representation (c) of the thermal annealed photoactive layer. The inset in (a) is the corresponding SAED pattern. The *arrow* is to indicate the increased intensity of (020) Debye-Scherrer ring from P3HT crystals compared to the SAED pattern. For Fig. 3c the *dash line* bordered regions represent the extension of existing P3HT crystals in the pristine film or newly developed PCBM-rich domain during the annealing step. Reprinted with permission from Yang et al. [153]. Copyright (2005), American Chemical Society

made from micrographs obtained from transmission electron microscopy. The authors investigated the blends of poly [2,7-(0,9-dioctyl-fluorene)-alt-5,5-(4',7'-di-2-thienyl-2',1'3'-benzothia-diazole)] (APFO-3) and PCBM. They used this method to supply a 3D representation of the morphology of the film, where domains with different scattering properties can be distinguished [154].

Marsh et al. employed sub-picosecond transient absorption (TA) spectroscopy on operating P3HT:PCBM devices to probe the effect of annealing on charge transfer dynamics and nanoscale morphology [155]. They removed the effect of high excitation densities which could otherwise dominate using their measurement configuration. The authors demonstrated that the charge transfer in pristine P3HT:PCBM devices proceeds on a sub-picosecond time scale. According to the authors, in annealed devices, annealing results in diffusion limited charge

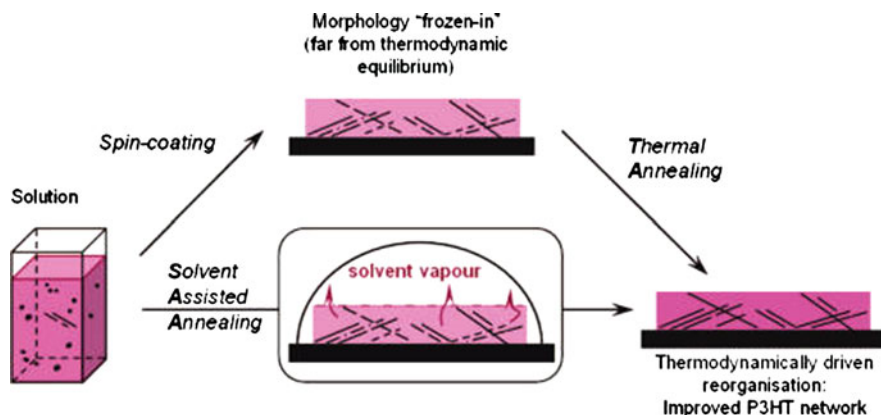


**Fig. 27** Morphology development in P3HT/PCBM photoactive layers depending on film preparation method. Reprinted with permission from Van Bavel et al. [143]. Copyright (2009), American Chemical Society

generation with a half time of ca. 3 ps, complete only after 30 ps. The authors address this as a result of exclusion of PCBM molecules and ordering of P3HT domains and correlated this with the improved PV efficiency [155].

Keawprajak et al. investigated the effect of a crystallizable solvent on the morphology and performance of BHJ solar cells based on a 1:1 weight-ratio RR-P3HT/PCBM blend, using chlorobenzene with different concentrations of 1,3,5-trichlorobenzene (TCB) as crystallizable aromatic solvents [156]. The authors demonstrated that the decelerated release of the residual solvent during the solidification of the blend film improves the self organization, and the surface of the film becomes smoother with the addition of TCB, which in turn improves organic/cathode contact. The authors concluded that the polymer blend film formed with a TCB crystallizable solvent exhibited better crystallinity, optical absorption, and polymer morphology than the polymer blend film formed without the TCB crystallizable solvent [156].

Polyfluorene copolymers are well known for their high charge carrier mobility, good processability, and high absorption coefficients. Among this class of polymers, poly[9,9'-dioctyl-fluorene-co-bithiophene] (F8T2) has excellent properties in both hole transport and thermotropic liquid crystallinity to allow better packing of the polymer via self assembly. The nanomorphological changes on the PV performance based on a F8T2:PCBM BHJ system were demonstrated by Huang et al. [157].

In summary, obtaining a desired morphology in polymer-fullerene composite solar cells is critical for device performance. Optimizing the electronic structure is not alone sufficient and there is not a direct recipe to apply to new material systems; therefore, morphology optimization should be performed for any combination of materials, where solvent selection is just one parameter among many [11].

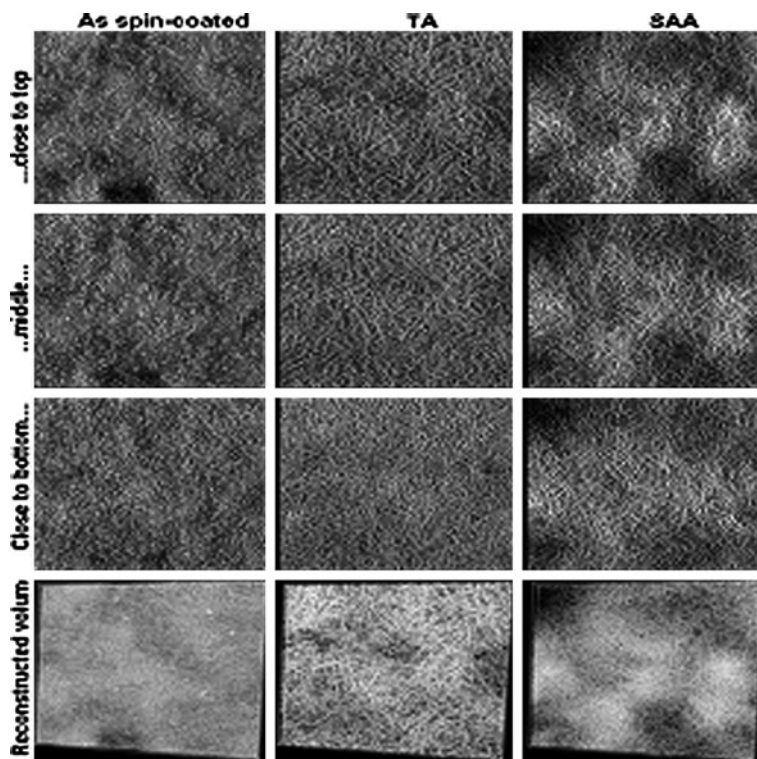
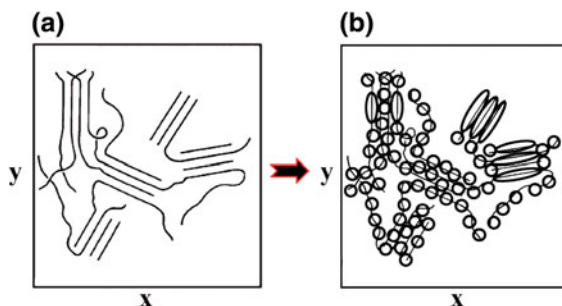


**Fig. 28** Results of EM applied to P3HT/PCBM photoactive layers: as spin-coated, thermally annealed at 130°C for 20 min (TA) and solvent assisted annealed for 3 h (SAA). The first three rows contain slices taken out of a reconstructed volume of the corresponding film. All slices are lying in the horizontal (X,Y) plane of the film at different depths (Z location): one slice close to the top of the film (i.e., close to the electron collecting LiF/Al electrode), another one in the middle of a film, and the third one close to the bottom of the film (near the hole collecting PEDOT:PSS/ITO electrode). The dimensions of the slices are around 1,700 nm × 1,700 nm. The images in the fourth row are snapshots of the corresponding film's reconstructed volume, i.e., a stack of all of the slices through the whole thickness of a film, with dimensions of around 1,700 nm × 1,700 nm × 100 nm. Reprinted with permission from Van Bavel et al. [143]. Copyright (2009), American Chemical Society

### 3.2 Charge Transport and Mobility

Charge carrier transport and mobility in organic semiconductors are of critical importance for the device performance of organic solar cells. There have been several studies on modeling the charge transport through organic solar cells. Depending on the degree of order, the charge carrier transport mechanism in organic solar cells falls between two extreme cases: band or hopping transport [77, 158]. For many systems, such as organic semiconductors it is not easy to determine which type of transport exists. Band transport is typically observed in highly

**Fig. 29** **a** Schematic description of polymer chains and **b** an illustration of how a long chain breaks into small conjugation units (or sites). Reproduced with permission from Tessler et al. [159]. Copyright Wiley-VCH Verlag GmbH&Co. KGaA.



purified molecular crystals at temperatures that are not too high [77]. For organic crystals, for example, it has been demonstrated that band transport dominates in the low  $T$  regime, while at room temperature hopping is the prevailing transport mechanism [158]. A characteristic feature of band transport, the temperature dependence follows power law behavior at lower temperatures. However, in the presence of traps, significant deviations from such behavior are observed [77]. In the other extreme case of an amorphous organic solid, hopping transport prevails, which leads to much lower mobility values. Instead of a power law temperature dependence, an activated behavior appears and the mobility also depends on the applied electric field. Furthermore, space charge and trapping effects as well as details of charge carrier injection mechanism have to be considered for describing electrical transport in organic solids [77]. Many studies based on the charge transport and mobility of organic semiconducting materials agree that most OPV materials investigated so far are disordered in nature. Introducing disorder into the lattice and breaking the crystal symmetry results in the wave functions becoming localized and the formation of energy states in the forbidden band gap. Therefore, former models describing the conductivity phenomenon in metals or other types of materials can no longer explain the transport under such circumstances. Since OPV materials are disordered in nature, the physical theories relating to the charge carriers through disordered media should be taken into account [159].

Tessler et al. suggested that a conjugated polymer cannot be considered a single electronic wire but rather as a wire broken into subunits by chemical or physical defects that are called conjugation units and the number of monomers making this unit is called the conjugation length (see Fig. 29) [159]. In this case, there are now many small electronic units that can also be thought of as small molecules distributed across the film. The only role that was played by the polymer chain was to determine the distribution of the units (“molecules”) in the film. With this simple picture, one can consider that there is a distribution of sites that can host charge and enable it to move across a film. Thus, one needs to analyze the charge transport across sites that are distributed in real space as well as in energy space according to their studies [159].

The key quantity that characterizes charge transport is the carrier mobility [160]. In the absence of any external potential, transport is purely diffusive and is

generally described by a simple diffusion equation. The application of an external electric field induces a drift of the charge carriers; the mobility can then be alternatively defined as the ratio between the velocity and the amplitude of the applied electric field. Diffusion should be seen as a local displacement of the charge around an average position, while drift induces a displacement of the average position. Drift is the effect that dominates the migration of the charges across an organic layer [160].

Even in the best cases, the charge mobilities of organic semiconductors are several orders of magnitude lower than those of inorganic PV materials. The low mobilities arise from the localization of electronic states on individual molecules or segments of molecules. Relatively weak intermolecular interactions mean that charge transport is best described by hopping transport rather than band transport [161]. There is extensive evidence from temperature and field dependent conductivity measurements that charge transport in both conjugated polymers and small molecules occurs by a hopping mechanism [77].

The requirement of balanced hole and electron mobilities is of critical importance for the device performance of organic solar cells. Low mobilities limit the performance of organic solar cells by enhancing the probability of charge recombination, limiting the charge separation yield, and increasing resistive losses [161]. Nelson et al. demonstrated that packing disorder can reduce mobility by several orders of magnitude for a disordered molecular semiconductor relative to the crystal. They mentioned that the effect of disorder on mobility is amplified by anisotropy in the orbitals involved in the charge transfer; side chains strongly influence mobility and transport in conjugated polymers is a function of both the extension of polymer chains and order in chain packing [161].

Charge carrier mobilities can be determined experimentally by using various techniques such as time of flight (TOF), field effect transistor (FET) configuration, charge extraction under linearly increasing voltage (CELIV), steady state current density–voltage response, admittance spectroscopy, and TRMC [160, 162]. Results from methods that measure mobilities under macroscopic distances ( $\approx 1$  mm) are often dependent on the purity and order in the material. Methods that measure mobilities over microscopic distances are less dependent on these characteristics [160].

As previously described, after photoinduced electron transfer at the donor/acceptor interface and dissociation, the electrons are localized in the PCBM phase whereas the holes remain in the PPV polymer chains. Then, the free electrons and holes must be transported via percolated PCBM and PPV pathways toward electrodes [163]. For pure PCBM, the electron mobility was reported as  $2 \times 10^{-7}$  m<sup>2</sup>/Vs [164], which is 4,000 times higher than the hole mobility in pristine MDMO-PPV, reported as  $5 \times 10^{-11}$  m<sup>2</sup>/Vs [165]. The hole mobility of pristine MDMO-PPV was rather low. Also, the results showed that usually the electron mobility and the hole mobility are unbalanced.

One of the ways to improve the charge carrier mobility in conjugated polymers is increasing the regioregularity of the conjugated backbone, as reported by Lutsen et al. [166]. However, fully regioregular MDMO-PPV lacked solubility, which is

quite important for OPV cells. Later, a soluble regiospecific (RS) MDMO-PPV was synthesized and the room temperature TOF mobility of this 70:30 RS-MDMO-PPV was found to be higher than the commercially available regiorandom RRa-MDMO-PPV [167].

Mozer et al. investigated the hole mobility of P3HT by the TOF technique and observed a negative electric field dependence of mobility for the first time in conjugated semiconducting polymers [168].

The question of interest was whether or not the mobility values of pristine materials changed upon blending. Melzer et al. demonstrated that the hole mobility in a 20:80 weight ratio MDMO-PPV:PCBM blend was enhanced by more than two orders of magnitude compared to the pure polymer value using space charge limited current (SCLC) measurements [169]. The difference between the electron and hole mobility was reduced by only a factor of 10, resulting in a more balanced transport [163].

The 2.5% efficient MDMO-PPV:PCBM-based solar cells make use of 80 wt% PCBM in the blend, a material which barely contributes to the absorption. Mih-aitchi et al. demonstrated that one of the main reasons for the relatively large amount of PCBM being required is the enhancement of the hole transport in MDMO-PPV, which is the slower carrier, when blended with PCBM [170]. An insufficient hole mobility will also lead to a build up of space-charge in the solar cell, which affects the fill factor and efficiency [171]. Therefore, an intrinsically higher hole mobility in the blend permits one to reduce the amount of PCBM and inhibits the occurrence of space charge, which will further increase the magnitude of the photogenerated current and enhance the PCE [170].

Among the factors that may influence charge transport in polymer-molecule or polymer-polymer blends are the different morphologies adopted by the two components, especially in the case where one is a high molecular weight polymer and the other is a small conjugated molecule [172]. Frost et al. studied the influence of polymer blend morphology on charge transport and photocurrent generation in polymer blends using Monte Carlo simulations. They reported that different morphologies, such as well dispersed, loosely coiled polymer chains (heterophilic) or aggregated, tightly coiled chains (homophilic) can be produced by varying the interaction energies between the chains with different types of process treatments, such as solvent or annealing. Frost et al. pointed out that the morphology strongly influences charge transport characteristics; that is, homophilic blends show a lower threshold for charge percolation and more dispersive transport than heterophilic blends, consistent with a higher probability of charge trapping in configurational traps. They explained the experimental observations, such as the effect of annealing on charge transients in some conjugated polymers, by their model in terms of process-induced changes in polymer morphology, whereas monomer-based transport models cannot explain the data [172]. They concluded that the morphology influences both transport and charge recombination such that the optimum composition and morphology is a sensitive function of charge recombination and separation rates and faster transport, achieved through

optimizing the blend morphology does not necessarily lead to higher photocurrent generation [172].

Pivrikas et al. reviewed the charge transport and recombination in polymer/fullerene organic solar cells [173]. They studied the transport and recombination in two polymer/fullerene mixtures: RR-P3HT/PCBM and MDMO-PPV/PCBM. They showed that the carrier mobility is strongly dependent on the film morphology and disorder. Therefore, charge carrier mobility can change orders of magnitude depending on film preparation techniques, solvents used for film deposition, time and temperature of the thermal treatment, etc. [173].

Shah et al. used a model to address the interplay between anisotropic charge transport and the orientational and/or crystalline ordering of donor molecules [174]. They presented the influence of the degree of ordering, the impact of ordering parallel or perpendicular to the electrodes, and the role of device thickness. They used a drift–diffusion model, which accounted for the effects of the anisotropic nature of charge transport in conjugated polymers and the donor–acceptor density inhomogeneities, to determine the PV performance. They tried to find answers for the following questions: “Is there an optimal degree of alignment influencing the efficiency of the solar cells?”, “Which among the parallel or perpendicular orientations (relative to the electrodes) of the molecules are more favorable for optimizing the efficiencies?”, and “What is the influence of anisotropic transport characteristics upon the optimal domain widths of the donor and acceptors?”. They considered “simulated morphologies” where alternating lamellae of donor and acceptor are aligned perpendicular to the two electrodes, forming an ordered heterojunction structure. They assumed that the donor molecules are aligned only either parallel or perpendicular to the interface to specifically elucidate the role of anisotropic charge transport. They characterized the degree of alignment by a scalar order parameter. According to their model, for perpendicularly aligned donors there exists an optimal degree of alignment to extract the best device efficiencies. In contrast, for the case of parallelly oriented donor molecules, they observed an opposite effect where stronger alignment is always better due to accompanying enhancement in transport to the electrodes. They observed that the magnitudes of short-circuit current density ( $J_{sc}$ ) are much smaller in the parallel orientation, reflecting the fact that the transport of excitons to the interface and subsequent dissociation is greatly diminished in this arrangement. For the interplay of the  $D$ – $A$  size with the anisotropic charge transport characteristics, Shah et al. commented that for the perpendicularly oriented donors, increasing the anisotropy enhances the exciton transport. In contrast, parallel-oriented donors are less affected by such anisotropies [174].

Ballantyne et al. used the TOF method to study the effect of P3HT molecular weight (MW) ( $M_n = 13$ – $121$  kDa) on the charge mobility in pristine and PCBM blend films using highly RR P3HT [175]. They observed a constant  $10^{-4}$  cm<sup>2</sup>/Vs mobility value as the molecular weight increased from 13–18 kDa, but the mobility value decreased by one order of magnitude as molecular weight further increased from 34–121 kDa. They showed that the decrease in charge mobility



observed in the blend films is accompanied by a change in surface morphology, and leads to a decrease in the performance of PV devices made from these blends. They attributed the decrease in mobility to the change in packing of the polymer chains. They mentioned that it is possible that high molecular weight chains become tangled, causing twisting of the polymer backbone, decreased intra-chain transport by creating more traps, and/or reduction of inter-chain charge hopping by allowing less overlap of conjugated segments. Combining their results, they proposed that there is an optimal P3HT molecular weight for charge transport and device performance between 13 and 34 kDa. Their modeling of the device behavior indicated that the effect of MW on device performance could not be explained solely in terms of differences in charge mobility. They mentioned that other factors, such as the effect of blend morphology on interface resistance, the effect of film thickness on transport, or the non-linear effect of transport on the net charge-generation rate, could be partly responsible for the variations in the efficiency [175].

In organic solar cells, the mobility simultaneously controls both the carrier extraction and the losses via carrier recombination [176]. Mandoc et al. demonstrated that the balance between carrier losses by extraction and by recombination leads to a distinct optimal carrier mobility with regard to the efficiency of organic solar cells [176]. They stated that for low mobilities, recombination losses limit the performance, whereas efficient extraction at high mobilities leads to a reduction in open-circuit voltage. The authors concluded that the maximal performance of the BHJ solar cells is governed by balancing transport and recombination and that both extremes of too low or too high mobility contribute to the loss of efficiency through different mechanisms. Therefore, an optimized carrier mobility is an important condition that must be fulfilled to obtain highly efficient organic solar cells [176].

In summary, low mobilities limit the performance of organic solar cells since the probability of charge recombination increases [161]. It should also be noted that using different methods to characterize the mobility may lead to very different mobility results. For example, when the hole mobility results of pristine P3HT are examined, the measured hole mobility ranges from  $10^{-8}$   $\text{m}^2/\text{Vs}$  in TOF and SCLC up to  $10^{-5}$   $\text{m}^2/\text{Vs}$  in FETs [177]. RR-P3HT self-organizes into a crystalline structure and, owing to the  $\pi$ - $\pi$  stacking direction, the charge (hole) transport is extremely efficient. Since in FET measurements the current travels in the plane of the film (parallel to the substrate), the anisotropy in the polymer-chain orientation contributes strongly to the difference in the measured mobility [177]. A different molecular weight of P3HT, the presence of PCBM, and/or the application of a thermal treatment will also affect the measured electron and hole mobilities [1, 178, 179]. Therefore, relevant values for charge carrier mobilities can only be obtained when measured in the same configuration and experimental conditions as used in an operational solar cell device [177].

## 4 Current Status of Solution Processed Conjugated Polymer-Based Organic Solar Cells

The first attempts to create organic solar cells were made by sandwiching a single layer of organic material between two electrodes of different work functions [180]. In these cells, the performance strongly depends on the nature of the electrodes.

In 1986, Tang realized a breakthrough by fabricating a bilayer organic PV cell using copper phthalocyanine and a perylene tetracarboxylic derivative [58]. A PVC of about 1% has been achieved under simulated AM2G illumination. A novel feature of the device was that the charge-generation efficiency was relatively independent of the bias voltage, resulting in cells with fill factor values as high as 0.65. The interface between the two organic materials, rather than the electrode/organic contacts, was found to be crucial in determining the PV properties of the cell [58]. Although this efficiency was a breakthrough at that time, the performance of this PV device was still limited since the only light absorption within a very thin layer close to the interface contributes to the photocurrent generation.

The carrier collection efficiency and PVC of polymer PV cells were improved by blending of the semiconducting polymer with  $C_{60}$  or its functionalized derivatives by Yu et al. [17]. Composite films of MEH-PPV and fullerenes exhibited efficiencies better than those that have been achieved with devices made with pure MEH-PPV by over two orders of magnitude. The efficient charge separation results from photoinduced electron transfer from the MEH-PPV (donor) to the  $C_{60}$  (acceptor); the high collection efficiency results from a bicontinuous network of internal donor–acceptor heterojunctions [17].

Halls et al. also showed that the interpenetrating network formed from a phase-segregated mixture of two semiconducting polymers provides both the spatially distributed interfaces necessary for efficient charge photo-generation, and the means for separately collecting the electrons and holes [5].

Various combinations of donor and acceptor materials have been used to fabricate BHJ solar cells. The most promising and successful combination of materials is a blend of a semiconducting polymer and a fullerene derivative as the acceptor. It was demonstrated that sub-picosecond charge transfer takes place at the interface of these materials, which ensures efficient charge generation [52].

A breakthrough on solution processed organic solar cells employing MDMO-PPV as the donor and PCBM as the acceptor was realized by Shaheen et al. [10]. They showed that the PCE of OPV devices based on a conjugated polymer/methanofullerene blend is dramatically affected by molecular morphology. By structuring the blend to be a more intimate mixture that contains less phase segregation of the methanofullerenes and simultaneously increasing the degree of interactions between conjugated polymer chains, they fabricated a device with a PVC of 2.5% under AM1.5G illumination. This was a nearly three-fold enhancement over previously reported values. The crucial step that improved the device performance was the use of a special solvent that improves the nanoscale morphology for charge generation and transport [10].

Although the efficiency of single-layer devices was improved by simple mixing the *p*- and *n*-type materials, this solution bears a new challenge. In the BHJ approach, the donor and acceptor components are mixed in a bulk volume so that each donor–acceptor interface is within a distance smaller than the exciton diffusion length of each absorbing site [43]. The donor and acceptor phases must form a bicontinuous and interpenetrating network. Therefore, bulk heterojunction devices are much more sensitive to the nanoscale morphology in the blend [43]. As previously discussed, to organize the donor and acceptor in a nanometer scale is a big challenge.

Further improvement in OPV efficiency was achieved when the PPV was replaced with P3HT. P3HT gave a further increase in the hole mobility and the PVC was improved to 3.5% [14].

Recently, polymer PV cells with PCEs approaching 5% were fabricated using titanium oxide ( $\text{TiO}_x$ ) as an optical spacer by Kim et al. [102]. In this study, solar cells with a  $\text{TiO}_x$  layer (deposited via a sol–gel process) between the active layer and the electron-collecting aluminum electrode exhibited approximately a 50% enhancement in short-circuit current compared to similar devices without the optical spacer, as a result of modification of the spatial distribution of the light intensity inside the device [102].

Konarka Technologies demonstrated a 5.21% power conversion efficient plastic solar cell with an active area of  $1.024 \text{ cm}^2$  (NREL certificate for Konarka solar cell from 11-20-2006) [181].

Park et al. demonstrated 6.1% efficient bulk heterojunction solar cells with internal quantum efficiency reaching 100% [25]. They fabricated devices using alternating copolymer, poly[*N*-9'-hepta-decanyl-2,7-carbazole-alt-5,5-(4',7'-di-2-thienyl-2',1',3'-benzothiadiazole)] (PCDTBT), in bulk heterojunction composites with the fullerene derivative [6,6]-phenyl  $\text{C}_{70}$ -butyric acid methyl ester (PC<sub>70</sub>BM). The PCDTBT/PC<sub>70</sub>BM solar cells exhibited a  $J_{\text{SC}}$  of  $10.6 \text{ mA cm}^{-2}$ , an  $V_{\text{OC}}$  of 0.88 V, a *FF* of 0.66 and a PCE of 6.1% under AM1.5G. The nearly 100% internal quantum efficiency implies that essentially every absorbed photon results in a separated pair of charge carriers and all photogenerated carriers are collected by the electrodes [25]. PCBM, which amounts to 80% of the photoactive layer, has a very low absorption coefficient in the visible region of the spectrum due to its symmetrically forbidden HOMO–LUMO transition. When the  $\text{C}_{60}$  moiety of [60]PCBM is replaced by a less symmetric fullerene, these transitions become slightly allowed and an increase in light absorption/harvesting is expected [11, 182].

Chen et al. showed that the open-circuit voltage of polymer solar cells constructed based on a low-bandgap polymer, PBDTTT, can be tuned, step by step using different functional groups to achieve values as high as 0.76 V [183]. This increased open-circuit voltage combined with a high short-circuit current density results in a polymer solar cell with a PVC as high as 6.77%, as certified by the National Renewable Energy Laboratory [183].

The demonstration of PCEs close to 8% under calibrated AM1.5G conditions demonstrates the potential of this technology. The fabrication using suitable

printing methods for the production of such organic solar cells is regarded as the next important milestone [181].

In terms of research trends, the main direction has been toward the achievement of high PCEs under simulated sunlight [184]. However, other important aspects include stability, cost and processing [184]. Long operational lifetimes of solar cells are required in real-life application. Polymer solar cells degrade under illumination and in the dark. Therefore, methods for enhancing the stability through the choice of better active materials, encapsulation, etc., are important [184].

## 5 Stability

Organic solar cells degrade under illumination and in the dark. Long operation lifetimes of solar cell devices are required in real-life applications and understanding the degradation mechanisms is of great importance for successful implementation of this promising technology [184]. For the technological development of organic solar cells, the important aspects aside from PCE are the stability, cost and processing [185, 186].

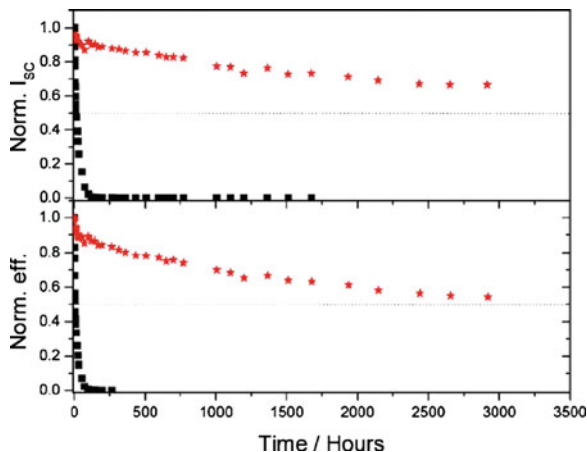
Organic materials are, by nature, more sensitive to chemical degradation, e.g., from oxygen and water, than inorganic materials. Diffusion of oxygen and water into the OPV device, photochemistry and photooxidation of polymers, degradation of a function of polymer preparation, and chemical degradation of the ITO electrode are seen as chemical degradation mechanisms whereas morphological stability can be seen as a physical degradation mechanism for OPV cells [184]. In a recent review by Jorgensen et al. these mechanisms are discussed [184]. The following points cause problems for the stability of devices [184]:

- Oxygen from the atmosphere will oxidize the organic layer, especially when the device is illuminated.
- Materials such as P3HT are less sensitive to this degradation. Annealing can lead to further structural changes when the devices are heated.
- Aluminium, which is the most commonly used metal electrode, reacts with oxygen and water and perhaps with the organic material due to its low work function.
- The transparent electrode, which is commonly ITO, is also not stable. Indium atoms pass to the organic layer and distribute themselves into the polymer layer.
- PEDOT:PSS layer is hygroscopic in nature and may bind to water.

These possible factors for degradation have various degrees of influence on the device lifetime.

Due to the degradation mechanisms mentioned above, polymer solar cells cannot operate in air for more than few hours. Therefore, appropriate encapsulation may help increase the lifetimes of these devices [112]. Dennler et al. reported a shelf lifetime study of MDMO-PPV:PCBM solar cells encapsulated in a new flexible and transparent poly(ethylene naphthalate) (PEN)-based ultra-high barrier

**Fig. 30** Normalized  $I_{SC}$  and efficiency of solar cells encapsulated with uncoated PET (black) and with the flexible gas barrier material (red) versus storage time in the dark under ambient air. Reprinted from [112] Copyright (2006) with permission from Elsevier



material fabricated entirely by plasma enhanced chemical vapor deposition (PECVD) [112]. They demonstrated that encapsulation raises the shelf lifetime (defined as the time performance degrades to 50% of the initial efficiency) of 30–57 mm<sup>2</sup> solar cells from a few hours to over 3,000 h, or more than 4 months [112].

Figure 30 shows the evolution of the normalized  $V_{OC}$  and FF of a typical solar cell versus storage time. In the case of PET encapsulation, both  $V_{OC}$  and FF decreased by 50% within less than 200 h. They observed that aging of the cells results in the development of a back diode that tends to drastically reduce FF. However, in the case of the flexible barrier encapsulation,  $V_{OC}$  remains at about 90% of its initial value after 3,000 h, as does FF (see Fig. 30) [112].

However, 3,000 h of device stability is not sufficient for this type of device in the market. MDMO-PPV is known to be particularly unstable and sensitive to aging. However, new materials, such as polythiophenes, that are much less sensitive to moisture and oxygen and allow even better PV conversion are becoming available [187]. The combination of such materials with this flexible gas barrier encapsulation might constitute a very promising advance in this field [112].

## 6 Technological Aspects of Organic Solar Cells

The technologically important features of organic solar cells can be summarized as following [185]:

- flexibility and transparency.
- potential to be manufactured in a continuous printing process.
- large area coating.
- easy integration in a wide variety of devices.
- cost-effectiveness.

- ecological and economic advantages.

These features are very important for commercialization. However, as in inorganic PV cells, OPV cells should also fulfill the basic requirements for renewable energy production [185].

The production aspects of OPV cells were reviewed by Brabec et al. [185]. They pointed out that there are three essential parameters for every solar technology to take its competitive position in the market: efficiency, lifetime, and cost per watt peak [185]. From efficiency point of view, a device efficiency of  $\sim 10\%$  and a module efficiency of  $\sim 5\%$  are regarded as critical market entry values. Higher efficiencies for OPV devices will demand novel materials, either low band gap materials or material combinations with better matched electronic levels, to improve  $I_{sc}$  and  $V_{oc}$ , respectively. From lifetime point of view, for low-cost devices, a life time of 3–5 years (operational life time of 3,000–5,000 h) is regarded as the market entry point. These values were derived from typical usage lifetimes of electronic goods that could potentially be powered by solar cells. According to Brabec et al., printing techniques are the necessary tool for significant cost reduction for PVs. Under the assumption that the material costs (including packaging and substrates) will further decrease with scale up, organic solar cells with a cost structure significantly below 1 USD/W<sub>p</sub> can be realized [185]. Brabec et al. foresee that the first applications will most likely be in consumer electronics: calculators, watches, sensors and innovative applications such as mobile phone chargers.

Compared to the efficiencies over 20% achieved by Si-PVs, the efficiency of OPV cells seem poor. However, other advantages, particularly the low cost, flexibility and easy integration into a wide variety of systems make them competitive for a range of applications such as packaging, smart fabrics, and signalization. Organic PVs utilize cheap and easy processing techniques, such as inkjet printing or spin coating, on large, flexible plastic substrates. The flexibility of the final product offers low weight and easy installation.

One company has already announced that plastic solar panels will be available for portable electronics, smart fabrics and building integrated PVs in the first quarter of 2011; they also added that customers interested in prototypes of plastic solar panels for portable electronics testing can obtain samples by mid-2010.

## 7 Conclusions

Recent milestones and improved efficiencies achieved by organic solar cells opened up a possibility for OPV devices to take their place in the market. The biggest advantages of organic-plastic solar cells are their low cost, flexibility and ability to be wrapped around structures or even applied like paint. As predicted by Scharber et al., PCEs of 10% are within the achievable range [30] and 15% can be achieved using the tandem solar cell concept [29]. Both of these efficiencies designate the development of novel donor materials.

Three key parameters will determine the success of organic solar cells: price, efficiency and lifetime. Since they are manufactured using rather simple techniques, their cost can be less than Si-based PV devices. The efficiencies achieved recently are considerable and encouraging, and the research continues for further improvement. Lifetime is a critical issue since organic materials are rather sensitive to oxygen and humidity. Since, full commercialization will take time, it is not easy to determine the product's lifetime of plastic solar cells.

The first commercial applications seem to be portable electronics and smart fabrics. It seems that the initial goal is not to replace the existing technology, such as solar panels used on rooftops.

From the scientific point of view, new donor and acceptor materials and possibly device concepts are needed for further efficiency improvement of organic solar cells. Several strategies can be summarized as the synthesis and development of low band gap materials for improved matching with the solar spectrum, synthesis and development of new electron accepting materials, tandem solar cells, improvement of hybrid solar cell and dye-sensitized solar cell concepts.

The ideal structure of BHJ solar cells requires that the two phases of donors and acceptors within the bulk heterojunction be spaced with an average separation of around 10–20 nm, equal or less than the exciton diffusion length. The two phases must be separated in percolated (ideally straight) pathways to ensure high mobility charge carrier transport with reduced recombination. Such a well organized nanostructure is not easy to obtain in classical polymer mixtures due to disorder. However, self organization of the organic semiconducting polymers (molecules) can be introduced using an amphiphilic structure di-block copolymer, which results in a self-organized phase [188], using supramolecular fullerene architectures by quadruple hydrogen bonding [189] and using uniaxially aligned, thin films of discotic columnar liquid crystalline materials [190].

Research on organic solar cells is highly interdisciplinary, promising, and challenging. The interdisciplinarity has already led to scientific and technological advancement since the organic solar cells are close to commercialization and is expected to lead to further achievements in this field.

## References

1. Ginley D, Green MA, Collins R (2008) Solar energy conversion toward 1 Terawatt. *MRS Bull* 33:355–363
2. Shockley W, Queisser HJ (1961) Detailed balance limit of efficiency of  $p-n$  junction solar cells. *J App Phys* 32:510–519
3. Poortmans J (2007) Organic solar cells: linking nanoscale to gigawatts? *Prog Photovolt Res App* 15:657–658
4. Minnaert B, Burgelman M (2007) Efficiency potential of organic bulk heterojunction solar cells. *Prog Photovolt Res App* 15:741–748
5. Halls JM, Walsh CA, Greenham NC et al (1995) Efficient photodiodes from interpenetrating polymer networks. *Nature* 376:498–500

6. Yu G, Heeger AJ (1995) Charge separation and photovoltaic conversion in polymer composites. *J App Phys* 78:4510–4515
7. Xue J, Uchida S, Rand BP et al (2004) 4.2% Efficient organic photovoltaic cells with low series resistances. *Appl Phys Lett* 84:3013–3015
8. Peumans P, Yakimov A, Forrest SR (2003) Small molecular weight organic thin-film photodetectors and solar cells. *J App Phys* 93:3693–3723
9. Thompson BC, Frechet JMJ (2008) Polymer-fullerene composite solar cells. *Angew Chem Int Ed* 47:58–77
10. Shaheen SE, Brabec C, Padinger F et al (2001) 2.5% efficient organic plastic solar cells. *Appl Phys Lett* 78:841–843
11. Wienk M, Kroon JM, Verhees WJH et al (2003) Efficient methano[70]fullerene/MDMO-PPV bulk heterojunction photovoltaic cells. *Angew Chemie Int Ed* 42:3371–3375
12. Chen T, Rieke RD (1992) The first regioregular head-to-tail poly(3-hexylthiophene-2, 5-diyl) and a regiorandom isopolymer: nickel versus palladium catalysis of 2(5)-bromo-5(2)-(bromozincio)-3-hexylthiophene polymerization. *J Am Chem Soc* 114:10087–10088
13. McCullough RD, Lowe RD, Jayaraman M et al (1993) Design, synthesis, and control of conducting polymer architectures: structurally homogeneous poly(3-alkylthiophenes). *J Org Chem* 58:904–912
14. Padinger F, Rittberger RS, Sariciftci NS (2003) Effects of post production treatment on plastic solar cells. *Adv Func Mat* 13:85–88
15. Chirvaze D, Parisi J, Hummelen JC et al (2004) Influence of nanomorphology on the photovoltaic action of polymer–fullerene composites. *Nanotechnology* 15:1317–1323
16. Ma WL, Yang CY, Gong X et al (2005) Thermally stable, efficient polymer solar cells with nanoscale control of the interpenetrating network morphology. *Adv Func Mat* 15:1617–1622
17. Yu G, Gao J, Hummelen JC et al (1995) Enhanced efficiencies via a network of internal donor-acceptor heterojunctions. *Science* 270:1789–1791
18. Sariciftci NS, Braun D, Zhang C et al (1993) Semiconducting polymer-buckminster fullerene heterojunctions: diodes, photodiodes and photovoltaic cells. *Appl Phys Lett* 62:585–587
19. Alem S, Bettignies R, Nunzi JM et al (2004) Efficient polymer based interpenetrated network photovoltaic cells. *Appl Phys Lett* 84:2178
20. Hummelen JC, Knight BW, LePeq F et al (1995) Preparation and characterization of fulleroid and methanofullerene derivatives. *J Org Chem* 60:532–538
21. Drechsel J, Maennig B, Kozlowski F et al (2004) High efficiency organic solar cells based on single or multi PIN structures. *Thin Solid Films* 451–452:515–517
22. Drechsel J, Maennig B, Gebeyehu D et al (2004) MIP-type organic solar cells incorporating phthalocyanine/fullerene mixed layers and doped wide-gap transport layers. *Org Electron* 5:175–186
23. Peumans P, Uchida S, Forrest SR (2003) Efficient bulk heterojunction photovoltaic cells using small-molecular-weight organic thin films. *Nature* 425:16–158
24. Peet J, Kim JY, Coates NE et al (2007) Efficiency enhancement in low-bandgap polymer solar cells by processing with alkane dithiols. *Nat Mater* 6(7):497–500
25. Park SH, Roy A, Beaupre S et al (2009) Bulk heterojunction solar cells with internal quantum efficiency approaching 100%. *Nat Photonics* 3(5):297–302
26. Kim Y, Cook S, Tuladhar S et al (2006) A strong regioregularity effect in self-organizing conjugated polymer films and high-efficiency polythiophene: fullerene solar cells. *Nat Mater* 5:197–203
27. Green M, Emery E, Hisikawa Y et al (2007) Solar cell efficiency tables. *Prog Photovolt Res Appl* 15:425–430
28. Dennler G, Scharber MC, Brabec CJ (2009) Polymer-fullerene bulk heterojunction solar cells. *Adv Mater* 21:1323–1338



29. Dennler G, Scharber MC, Ameri T et al (2008) Design rules for donors in bulk-heterojunction tandem solar cells? Towards 15% energy-conversion efficiency. *Adv Mater* 20:579–583
30. Scharber MC, Mühlbacher D, Koppe M et al (2006) Design rules for donors in bulk heterojunction solar cells-towards 10% energy conversion efficiency. *Adv Func Mat* 18:789–794
31. Servaites JD, Yeganeh S, Marks TJ et al (2010) Efficiency enhancement in organic photovoltaic cells: consequences of optimizing series resistance. *Adv Func Mat* 20:97–104
32. Wang X, Liu D, Li J (2010) Organic photovoltaic materials and thin film solar cells. *Front Chem China* 5:45–60
33. Huynh WU, Dittmer JJ, Alivisatos AP (2002) Hybrid nanorod polymer solar cells. *Science* 295:2425–2427
34. Coakley KM, McGehee MD (2003) Photovoltaic cells made from conjugated polymers infiltrated into mesoporous Titania. *Appl Phys Lett* 83:3380–3383
35. Kim JY, Lee K, Coates NE et al (2007) Efficient tandem polymer solar cells fabricated by all-solution processing. *Science* 317:222–225
36. Wienk MM, Turbiez MGR, Struijk MK et al (2006) Low-band gap poly(di-2 thienylthienopyrazine):fullerene solar cells. *Appl Phys Lett* 88:153511–153514
37. Hou J, Chen HY, Zhang S et al (2008) Synthesis, characterization, and photovoltaic properties of a low band gap polymer based on silole-containing polythiophenes and 2, 1, 3-benzothiadiazole. *J Am Chem Soc* 130:16144–16145
38. Koetse MM, Sweelsson J, Hoekerd KT et al (2006) Efficient polymer:polymer bulk heterojunction solar cells. *Appl Phys Lett* 88:083504–083507
39. Tada K, Hirohata, Hosada M et al (1997) Donor polymer (PAT6)—acceptor polymer (CNPPV) fractal network photocells. *Synth Met* 85:1305–1306
40. Liao H, Chen LM, Xu Z et al (2008) Highly efficient inverted polymer solar cell by low temperature annealing of CS<sub>2</sub>CO<sub>3</sub> interlayer. *Appl Phys Lett* 92:173303–173306
41. Katz EA, Gevorgyan S, Orynbayev MS et al (2007) Outdoor testing and long-term stability of plastic solar cells. *Eur Phys J Appl Phys* 36:307–311
42. Hauch JA, Schilinsky P, Choulis SA et al (2008) Flexible organic P3HT:PCBM bulk heterojunction modules with more than 1 year outdoor lifetime. *Solar Energy Mater Solar Cells* 92:727–731
43. Hoppe H, Sariciftci NS (2004) Organic solar cells: an overview. *J Mater Chem* 19:1924–1945
44. Heeger AJ (2001) Nobel lecture: semiconducting and metallic polymers: the fourth generation of polymeric materials. *Rev Mod Phys* 73:681–700
45. Borroughes JH, Bradley DDC, Brown AR et al (1990) Light emitting diodes based on conjugated polymers. *Nature* 347:539–541
46. Berggren M, Gustafsson G, Inganäs O et al (1994) Green electroluminescence in Poly-(3-cyclohexylthiophene) light-emitting diodes. *Adv Mater* 6:488–490
47. Gadisa A, Person E, Andersson MR et al (2007) Red and near infrared polarized light emissions from polyfluorene copolymer based light emitting diodes. *Appl Phys Lett* 90:113510–113513
48. Bao Z, Dodabalapur A, Lovinger A et al (1996) Soluble and processable regioregular poly(3-hexylthiophene) for thin film field-effect transistor applications with high mobility. *Appl Phys Lett* 69:4108–4111
49. Sirringhaus H, Tessler N, Friend RH (1998) Integrated optoelectronic devices based on conjugated polymers. *Science* 280:1741–1744
50. Neugebauer H, Brabec C, Hummelen JC, Sariciftci NS (2000) Stability and photodegradation mechanisms of conjugated polymer/fullerene plastic solar cells 61:35–42
51. Kanicki J (1986) *Handbook of conducting polymers* Marcel Dekker, New York, p 544
52. Sariciftci NS, Smilowitz L, Heeger AJ et al (1992) Photoinduced electron transfer from a conducting polymer to buckminsterfullerene. *Science* 258:1474–1476

53. Smilowitz L, Sariciftci NS, Wu R et al (1993) Photoexcitation spectroscopy of conducting-polymer-C<sub>60</sub> composites: photoinduced electron transfer. *Phys Rev B* 47:13835–13842
54. Kraabel B, Hummelen JC, Vacar D et al (1996) Subpicosecond photoinduced electron transfer from conjugated polymers to functionalized fullerenes. *J Chem Phys* 104:4267–4274
55. Morita S, Zakhidov AA, Yoshino K (1992) Doping effect of Buckminsterfullerene in conducting polymer: change of absorption spectrum and quenching of luminescence. *Solid State Commun* 82:249–252
56. Yoshino K, Yin XH, Morita S et al (1993) Enhanced photoconductivity of C<sub>60</sub> doped Poly(3-alkylthiophene). *Solid State Commun* 85:85–88
57. Wudl F (1992) The chemical properties of Buckminsterfullerene (C<sub>60</sub>) and the birth and infancy of fulleroids. *Acc Chem Res* 25:157–161
58. Tang CW (1986) Two layer organic photovoltaic cell. *App Phys Lett* 43:183–186
59. Heremans P, Cheyng D, Rand BP (2009) Strategies for increasing the efficiency of heterojunction organic solar cells: material selection and device architecture. *Acc Chem Res* 42:1740–1747
60. Archer M, Hill R (2001) Clean electricity from photovoltaics. Imperial College Press, London
61. Würfel P (2007) Photovoltaic principles and organic solar cells. *Chimia* 61:770–774
62. Haugeneder A, Neges M, Kallinger C et al (1999) Exciton diffusion and dissociation in conjugated polymer/fullerene blends and heterostructures. *Phys Rev B* 59:15346–15351
63. Theander M, Yartsev A, Zigmantas D et al (2000) Photoluminescence quenching at a polythiophene/C<sub>60</sub> heterojunction. *Phys Rev B* 61:12957–12963
64. Stübinger T, Brütting W (2001) Exciton diffusion and optical interference in organic donor/acceptor photovoltaic cells. *J Appl Phys* 90:3632–3642
65. Mozer A, Sariciftci NS (2006) Conjugated polymer photovoltaic devices and materials. *C R Chimie* 9:568–577
66. Gregg BA, Hanna MC (2003) Comparing organic to inorganic photovoltaic cells: theory, experiment, and simulation. *J Appl Phys* 93:3605–3614
67. Popovic ZD, Hor A, Loutfy R (1988) A study of carrier generation mechanism in benzimidazole perylene/tetraphenyldiamine thin film structures. *Chem Phys* 127:451–457
68. Arkhipov V, Emelianova EV, Baessler (1999) Hot exciton dissociation in a conjugated polymer. *Phys Rev Lett* 82:1321–1324
69. Koster LJA, Smits ECP, Mihaiilechi VD et al (2005) Device model for the operation of polymer/fullerene bulk heterojunction solar cells. *Phys Rev B* 72:085205–085214
70. Na S, Kim S, Jo J et al (2008) Efficient and flexible ITO free organic solar cells using highly conductive polymer anodes. *Adv Mater* 20:4061–4067
71. Cui J, Wang A, Edleman NL et al (2001) Indium tin oxide alternatives—high work function transparent conducting oxides as anodes for organic light-emitting diodes. *Adv Mater* 13:1476–1480
72. Rowell MW, Topinka MA, McGehee MA et al (2006) Organic solar cells with carbon nanotube network electrodes. *Appl Phys Lett* 88:233506–233509
73. Frohne H, Shaheen S, Brabec C et al (2002) Influence of anodic work function on the performance of organic solar cells. *Chem Phys Chem* 3:795–799
74. Zhang F, Johansson M, Andersson MR et al (2002) Polymer photovoltaic cells with conducting polymer anodes. *Adv Mater* 14:662–665
75. Huang J, Miller PF, Wilson JS et al (2005) Investigation of the effects of doping and post-deposition treatments on the conductivity, morphology, and work function of poly(3,4-ethylenedioxythiophene)/poly(styrene sulfonate) films. *Adv Func Mater* 15:290–296
76. Hiramoto M, Fujiwara H, Yokoyama M et al (1991) Three-layered organic solar cell with a photoactive interlayer of codeposited pigments. *Appl Phys Lett* 58:1062–1065
77. Brütting W (2006) Introduction to physics of organic semiconductors in physics of organic semiconductor. pp 1–12, Wiley-VCH, Weinheim. [10.1002/3527606637](https://doi.org/10.1002/3527606637)

78. Geens W, Aernouts T, Poortmans J et al (2002) Organic co-evaporated films of a PPV-pentamer and C<sub>60</sub>: model systems for donor/acceptor polymer blends. *Thin Solid Films* 403–404:438–443
79. Tsuzuki TT, Shirota J, Rostalski J et al (2000) The effect of fullerene doping on photoelectric conversion using titanyl phthalocyanine and a perylene pigment. *Sol Energy Mater Sol Cells* 61:1–8
80. Brabec CJ, Shaheen SE, Winder C et al (2002) Effect of LiF/metal electrodes on the performance of plastic solar cells. *App Phys Lett* 80:1288–1291
81. Hung LS, Tang CW, Mason NG (1997) Enhanced electron injection in organic electroluminescence devices using an Al/LiF electrode. *App Phys Lett* 70:152–155
82. Jabbour GE, Kawahe Y, Shaheen S et al (1997) Highly efficient and bright organic electroluminescent devices with an aluminum cathode. *Appl Phys Lett* 71:1762–1765
83. Jong D, Friedlein MP, Osikowicz RW et al (2006) Ultraviolet photoelectron spectroscopy of polymers. *Mol Cryst Liq Cryst* 455:193–203
84. Parker I (1994) Carrier tunneling and device characteristics in light emitting diodes. *J Appl Phys* 75:1656–1667
85. Horowitz G (1990) Organic semiconductors for new electronic devices. *Adv Mater* 2:287–292
86. Glenis S, Tourillon G, Garnier F (1984) Electrochemically grown polythiophene and Poly(3-methylthiophene) organic photovoltaic cells. *Thin Solid Films* 111:93–103
87. Braun D, Heeger AJ (1991) Visible light emission from semiconducting polymer diodes. *Appl Phys Lett* 58:1982–1985
88. Yu G, Zhang C, Heeger AJ (1994) Dual function semiconducting polymer devices light emitting and photodetecting diodes. *Appl Phys Lett* 64:154–1540
89. Antoniadis H, Hsieh BR, Abkowitz MA et al (1994) Photovoltaic and photoconductive properties of aluminum/poly(p-phenylene vinylene) interfaces. *Synth Metals* 62:265–271
90. Hoppe H, Sariciftci NS (2008) Polymer solar cells. *Adv Poly Sci Springer Berlin Heidelberg* 1–86
91. Brabec CJ, Sariciftci NS, Hummelen JC (2001) Plastic solar cells. *Adv Func Mater* 11:15–26
92. Yamashita Y, Takashima W, Kaneto K (1993) Characteristics of heterojunction diode of C<sub>60</sub>/tetratiafulvalene (TTF). *Jpn J Appl Phys* 32:L1017–L1020
93. Halls JJM, Friend R (1997) The photovoltaic effect in a poly(p-phenylenevinylene)/perylene heterojunction. *Synth Met* 85:1307–1308
94. Peumans P, Forrest SR (2001) Very-high-efficiency double-heterostructure copper phthalocyanine/C<sub>60</sub> photovoltaic cells. *Appl Phys Lett* 79:126–129
95. Van Duren JKJ, Yang XN, Loos J et al (2004) Relating the morphology of Poly(p-phenylene vinylene)/methanofullerene blends to solar-cell performance. *Adv Func Mat* 14:425–434
96. Martens T, Dhaen J, Munters T et al (2003) Disclosure of the nanostructure of MDMO-PPV:PCBM bulk hetero-junction organic solar cells by a combination of SPM and TEM). *Synth Met* 138:243–247
97. Mihailetchi VD, Blom PWM, Hummelen JC et al (2003) Cathode dependence of the open-circuit voltage of polymer:fullerene bulk heterojunction solar cells. *J Appl Phys* 94:6849–6855
98. Brabec CJ, Cravino A, Meissner D et al (2001) Origin of the open circuit voltage of plastic solar cells. *Adv Func Mat* 11:374–380
99. Mihailetchi VD, Koster LJA, Blom PWM (2004) Effect of metal electrodes on the performance of polymer:fullerene bulk heterojunction solar cells. *Appl Phys Lett* 85:970–973
100. Hoppe H, Niggemann M, Winder C et al (2004) Nanoscale morphology of conjugated polymer/fullerene based bulk heterojunction solar cells. *Adv Func Mat* 14:1005
101. Schilinsky P, Waldauf C, Brabec CJ (2002) Recombination and loss analysis in polythiophene based bulk heterojunction photodetectors. *Appl Phys Lett* 81:3885–3888

102. Kim JY, Kim SH, Lee HH et al (2006) New architecture for high efficiency polymer photovoltaic cells using solution based titanium oxide as an optical spacer. *Adv Mat* 18:572–576
103. Spanggaard H, Krebs F (2004) A brief history of the development of organic and polymeric photovoltaics. *Sol Energy Mater Sol Cells* 83:125–146
104. Rostalski J, Meissner D (2000) Monochromatic versus solar efficiencies of organic solar cells. *Sol Energy Mater Sol Cells* 61:87–95
105. Shrotriya V, Li G, Yao Y et al (2006) Accurate measurement and characterization of organic solar cells. *Adv Func Mat* 16:2016–2023
106. Dutta U, Chatterjee P (2004) The open circuit voltage in amorphous silicon p-i-n solar cells and its relationship to material, device and dark diode parameters. *J Appl Phys* 96:2261–2272
107. Marks RN, Halls JJM, Bradley DDC et al (1994) The photovoltaic response in poly(p-phenylene vinylene) thin film devices. *J Phys Condens Matter* 6:1379–1394
108. Cravino A, Schilinsky P, Brabec C (2007) Characterization of organic solar cells: the importance of device layout. *Adv Func Mat* 17:3906–3910
109. Kim M-S, Kang M-G, Guo L-J et al (2008) Choice of electrode geometry for accurate measurement of organic photovoltaic cell performance. *Appl Phys Lett* 92:133301–133304
110. Li G, Shrotriya V, Huang J et al (2005) High-efficiency solution processable polymer photovoltaic cells by self-organization of polymer blends. *Nat Mater* 4:864–868
111. Miller S, Fanchini G, Lin Y-Y et al (2008) Investigation of nanoscale morphological changes in organic photovoltaics during solvent vapor annealing. *J Mater Chem* 18:306–312
112. Dennler G, Lungenschmied C, Neugebauer H et al (2006) A new encapsulation solution for flexible organic solar cells. *Thin Solid Films* 511:349–353
113. Koster LJA, Mihailetschi VD, Ramaker R et al (2005) Light intensity dependence of open circuit voltage of polymer:fullerene solar cells. *Appl Phys Lett* 86:123509–123512
114. Malliaras GG, Salem JR, Brock PJ et al (1998) Photovoltaic measurement of the built-in potential in organic light emitting diodes and photodiodes. *J Appl Phys* 84:1583–1588
115. Gregg B (2003) Excitonic solar cells. *J Phys Chem B* 107:4688–4698
116. Ramsdale CM, Barker JA, Arias AC et al (2002) The origin of the open circuit voltage in polyfluorene-based photovoltaic devices. *J Appl Phys* 92:4266–4271
117. Antoniadis H, Hsieh BR, Abkowitz MA et al (1993) Photovoltaic properties of poly(p-phenylenevinylene/aluminum interfaces). *Polymer Preprints. Polymer preprints* 34:490–491
118. Karg S, Riess W, Dyakonov V et al (1993) Electrical and optical characterization of poly(phenylene-vinylene) light emitting diodes. *Synth Met* 54:427–433
119. Gadisa A, Svensson M, Andersson MR et al (2004) Correlation between oxidation potential and open circuit voltage of composite solar cells based on blends of polythiophenes/fullerene derivative. *Appl Phys Lett* 84:1609–1612
120. Liu J, Shi Y, Yang Y (2001) Solvation induced morphology effects on the performance of polymer-based photovoltaic devices. *Adv Func Mat* 11:420–424
121. Soci C, Hwang IW, Moses D et al (2007) Photoconductivity of a low-bandgap conjugated polymer. *Adv Func Mat* 17:632–636
122. Nunzi JM (2002) Organic photovoltaic materials and devices. *C R Physique* 3:523–542
123. Winder C, Sariciftci NS (2004) Low band gap polymers for photon harvesting in bulk heterojunction solar cells. *J Mat Chem* 14:1077–1086
124. Campos L, Tontcheva A, Günes S et al (2005) Extended photocurrent spectrum of a low band gap polymer in a bulk heterojunction solar cell. *Chem Mater* 17:4031–4033
125. Perzon E, Wang X, Admassic S et al (2006) An alternating low band-gap polyfluorene for optoelectronic devices. *Polymer* 47:4261–4268
126. Cravino A, Loi M, Scharber M et al (2003) Spectroscopic properties of PEDOTEHIITNA novel soluble low band-gap conjugated polymer. *Synth Met* 137:1435–1436
127. Wienk M, Struijk M, Janssen R (2006) Low band gap polymer bulk heterojunction solar cells. *Chem Phys Lett* 422:488–491

128. Bundgaard E, Krebs F (2006) Low-band-gap conjugated polymers based on thiophene, benzothiadiazole, and benzo-bis(thiadiazole). *Macromolecules* 39:2823–2831
129. Bundgaard E, Krebs F (2007) Large-area photovoltaics based on low band gap copolymers of thiophene and benzothiadiazole or benzo-bis(thiadiazole). *Sol Energy Mater Sol Cells* 91:1019–1025
130. Winder C, Matt G, Hummelen JC et al (2002) Sensitization of low bandgap polymer bulk heterojunction solar cells. *Thin Solid Films* 403–404:373–379
131. Bundgaard E, Krebs F (2007) Low band gap polymers for organic photovoltaics. *Sol Energy Mater Sol Cells* 91:954–985
132. Moule AJ, Bonekamp BJ, Meerholtz K (2006) The effect of active layer thickness and composition on the performance of bulk heterojunction solar cells. *J Appl Phys* 100:094503–094510
133. Hoppe H, Sariciftci NS, Meissner D (2003) Modeling the optical absorption within conjugated polymer/fullerene-based bulk-heterojunction organic solar cells. *Sol Energy Mater Sol Cells* 80:105–113
134. Peumans P, Bulovic V, Forrest SR (2000) Efficient photon harvesting at high optical intensities in ultrathin organic double-heterostructure photovoltaic diodes. *Appl Phys Lett* 76:2650–2653
135. Roman LS, Inganaes O, Nyberg T et al (2000) Trapping light in polymer photodiodes with soft embedded gratings. *Adv Mat* 12:189–195
136. Delley B, Kiess H (1994) 2-dimensional simulation of high efficiency silicon solar cells. *Sol Energy Mater Sol Cells* 33:1–10
137. Niggemann M, Glatthaar M, Gombert A et al (2004) Diffraction gratings and buried nano-electrodes-architectures for organic solar cells. *Thin Solid Films* 451–452:619–623
138. Gupta D, Mukhopadhyay S, Narayan K S (2010) Fill factors in organic solar cells. *solar energy materials and solar cells*. 94:1309–1313
139. M-Su Kim, B-Gi Kim, Kim J (2009) Effective variables to control the fill factor of organic photovoltaic cells. *Appl Mater Interf* 1:1264–1269
140. Barrau S, Andersson V, Zhang F et al (2009) Nanomorphology of bulk heterojunction organic solar cells in 2D and 3D correlated to photovoltaic performance. *Macromolecules* 42:4646–4650
141. Maturova K, Van Bavel SS, Wienk MM et al (2009) Morphological device model for organic bulk heterojunction solar cells. *Nano Lett* 9:3032–3037
142. Markov DE, Hummelen JC, Blom PWM et al (2005) Dynamics of exciton diffusion in poly(*p*-phenylene vinylene)/fullerene heterostructures. *Phys Rev B* 72:045216–045221
143. Van Bavel SS, Sourty E, De With G et al (2009) Three dimensional nanoscale organization of bulk heterojunction polymer solar cells. *Nano Lett* 9:507–513
144. Ahn T, Sein HHHH (2002) Effect of annealing of polythiophene derivative for polymer light-emitting diodes. *Appl Phys Lett* 80:392–395
145. Brown PJ, Thomas DS, Köhler A et al (2003) Effect of interchain interactions on the absorption and emission of poly(3-hexylthiophene). *Phys Rev B* 67:064203–064219
146. Nakazono M, Kawai T, Yoshino K et al (1994) Effects of heat treatment on properties of poly(3-alkyl)thiophene. *Chem Mater* 6:864–870
147. Zhang F, Svensson M, Andersson M et al (2001) Soluble polythiophenes with pendant fullerene groups as double cable materials for photodiodes. *Adv Mat* 13:1871–1874
148. Mattis B A, Chang P C, Subramarian V (2003) Effect of thermal cycling on the performance of poly(3-hexyl)thiophene transistors. *Mater Res Soc Symp Proc* 771 L.10.35.1
149. Li G, Shrotriya V, Yang Y (2005) Investigation of annealing effects and film thickness dependence of polymer solar cells based on poly (3-hexylthiophene). *J Appl Phys* 98:043704–043709
150. Al-Ibrahim M, Ambacher O, Sensfuss S (2005) Effects of solvent and annealing on the improved performance of solar cells based on poly(3-hexyl)thiophene. *Fullerene* 86:201120–201123

151. Erb T, Zhokhavets U, Gobsh G et al (2005) Correlation between structural and optical properties of composite polymer/fullerene films for organic solar cells. *Adv Func Mat* 15:1193–1196
152. Savenije TJ, Kroeze JE, Yang X et al (2005) The effect of thermal treatment on the morphology and charge carrier dynamics in a polythiophene-fullerene bulk heterojunction. *Adv Func Mat* 15:1260–1266
153. Yang X, Loos J, Veenstra SC et al (2005) Nanoscale morphology of high-performance polymer solar cells. *Nanoletters* 5:579–583
154. Andersson V, Herland A, Masich S et al (2009) Imaging of the 3D nanostructure of a polymer solar cell by electron tomography. *Nano Lett* 9:853–855
155. Marsh RA, Hodgkiss JM, Seifried SA et al (2010) Effect of annealing on P3HT:PCBM charge transfer and nanoscale morphology probed by ultrafast spectroscopy. *Nano Lett* 10:923–930
156. Keawprajak A, Piyakulawat P, Klamchuen A et al (2010) Influence of crystallizable solvent on the morphology and performance of P3HT:PCBM bulk heterojunction solar cells. *Sol Energy Mater Sol Cells* 94:531–536
157. Huang JH, Ho ZY, Kekuda D et al (2009) Effects of nanomorphological changes on the performance of solar cells with blends of poly[9, 9'-dioctyl-fluorene-co-bithiophene] and a soluble fullerene. *Nanotechnology* 20:025202–025211
158. Ortmann F, Bechstedt F, Karsten H (2010) Charge transport in organic crystals: interplay of band transport, hopping and electron-phonon scattering. *New J Phys* 12:023011. doi: [10.1088/1367-2630/12/2/023011](https://doi.org/10.1088/1367-2630/12/2/023011)
159. Tessler N, Preezant Y, Rappaport N et al (2009) Charge transport in disordered organic materials and its relevance to thin film devices. *Adv Mater* 21:2741–2761
160. Coropceanu V, Cornil J, Filho DAS et al (2007) Charge transport in organic semiconductors. *Chem Rev* 107:926–952
161. Nelson J, Kwiatkowski JJ, Kirkpatrick J et al (2009) Modeling charge transport in organic photovoltaic materials. *Acc Chem Res* 42:1768–1778
162. Karl N (2003) Charge carrier transport in organic semiconductors. *Synth Met* 133–134:649–657
163. Blom PWM, Mihailitchi VD, Koster LJA et al (2007) Device physics of polymer:fullerene bulk heterojunction solar cells. *Adv Mater* 19:1551–1566
164. Mihailitchi VD, van Duren JKJ, Blom PWM et al (2003) Electron transport in a methanofullerene. *Adv Func Mat* 13:43–46
165. Blom PWM, de Jong MJM, van Munster MG (1997) Electric-field and temperature dependence of the hole mobility in poly(p-phenylene vinylene). *Phys Rev B* 55:R656–R659
166. Lutsen L, Adriaenssens, Becker H et al (1999) New synthesis of a soluble high molecular weight poly(arylene vinylene): poly[2-methoxy-5-(3, 7-dimethyloctyloxy)-p-phenylene vinylene] polymerization and device properties. *Macromolecules* 32:6517–6525
167. Mozer AJ, Denk P, Scharber MC et al (2004) Novel regiospecific MDMO–PPV copolymer with improved charge transport for bulk heterojunction solar cells. *J Phys Chem B* 108:5235–5242
168. Mozer A, Sariciftci NS (2004) Negative electric field dependence of charge carrier drift mobility in conjugated, semiconducting polymers. *Chem Phys Lett* 389:438–442
169. Melzer C, Koop E, Mihailitchi VD et al (2004) Hole transport in poly(phenylene vinylene)/methanofullerene bulk-heterojunction solar cells. *Adv Func Mater* 14:865–870
170. Mihailitchi VD, Koster LJA, Blom PWM et al (2005) Compositional dependence of the performance of poly(p-phenylene vinylene): methanofullerene bulk-heterojunction solar cells. *Adv Func Mater* 15:795–801
171. Mihailitchi VD, Wildeman J, Blom PWM (2005) Space-charge limited photocurrent. *Phys Rev Lett* 94:126602–126606
172. Frost JM, Cheynis F, Tuladhar SM et al (2006) Influence of polymer-blend morphology on charge transport and photocurrent generation in donor-acceptor polymer blends. *Nano Lett* 6:1674–1681

173. Pivrikas A, Sariciftci NS, Juska G et al (2007) A review of charge transport and recombination in polymer/fullerene organic solar cells. *Prog Photovolt Res Appl* 15:677–696
174. Shah M, Pryamitsyn V, Ganesan V (2009) Effect of anisotropic charge transport on device characteristics of polymer solar cells. *Appl Phys Lett* 95:194101–194104
175. Ballantyne AM, Chen L, Dane J et al (2008) The effect of poly(3-hexyl)thiophene (P3HT) molecular weight on charge transport and the performance of polymer:fullerene solar cells. *Adv Func Mater* 18:2373–2380
176. Mandoc MM, Koster LJA, Blom PWM (2007) Optimum charge carrier mobility in organic solar cells. *Appl Phys Lett* 90:133504–133507
177. Mihailetchi VD, Xie H, Boer de B et al (2006) Charge transport and photocurrent generation in poly(3-hexylthiophene):methanofullerene bulk-heterojunction solar cells. *Adv Func Mater* 16:699–708
178. Kline RJ, McGehee MD, Kadnikova EN et al (2003) Controlling the field effect mobility of regioregular polythiophene by changing the molecular weight. *Adv Mater* 15:1519–1522
179. Goh C, Kline RJ, McGehee MD et al (2005) Molecular-Weight-Dependent Mobilities in Regioregular Poly (3-hexyl-thiophene) Diodes. *Appl Phys Lett* 86:122110–122112
180. Chamberlain GA (1983) Organic solar cells: a review. *Solar Cells* 8:47–83
181. Hoth CN, Choulis SA, Schilinsky P et al (2007) High photovoltaic performance of inkjet printed polymer:fullerene blends. *Adv Mater* 19:3973–3978
182. Arbogast JW, Foote CS (1991) Photophysical properties of C70. *J Am Chem Soc* 113:8886–8889
183. Chen H-Y, Hou J, Zhang S et al (2009) Polymer solar cells with enhanced open-circuit voltage and efficiency. *Nat Photonics* 3:649–653
184. Jorgensen M, Norrman K, Krebs FC (2008) Stability and degradation of polymer solar cells. *Sol Energy Mater Sol Cells* 92:686–714
185. Brabec CJ, Hauch JA, Schilinsky P et al (2005) Production aspects of organic photovoltaics and their impact on the commercialization of devices. *MRS Bull* 30:50–52
186. Krebs FC (2005) Alternative PV: large scale organic photovoltaics. *Refocus* 6:38–39
187. Schuller S, Schilinsky P, Hauch J et al (2004) Determination of the degradation constant of bulk heterojunction solar cells by accelerated lifetime measurements. *Appl Phys A* 79:37–40
188. Jenekhe S, Chen XL (1998) Self-assembled aggregates of rod-coil block copolymers and their solubilization and encapsulation of fullerenes. *Science* 279:1903
189. Rispens MT, Sanchez L, Beckers EHA et al (2003) Supramolecular fullerene architectures by quadruple hydrogen bonding. *Synth Met* 135:801–803
190. Tracz A, Jeszka JK, Watson MD et al (2003) Uniaxial alignment of the columnar superstructure of a hexa (Alkyl) hexa-*peri*-hexabenzocoronene on untreated glass by simple solution processing. *J Am Chem Soc* 125:1682–1683